An Assessment of Precision Gamma Scanning for Inspecting WR Fuel Rods

EPRI

EPRI NP-1952
Project 1702-4
Final Report
July 1981

Keywords:
Gamma Scanning
Fuel Performance
Fission Products
Nondestructive Testing

Prepared by
Los Alamos Scientific Laboratory
Los Alamos, New Mexico

ELECTRIC POWER RESEARCH INSTITUTE

DISCLAIMER

An Assessment of Precision Gamma Scanning for Inspecting LWR Fuel Rods

NP-1952
Research Project 1702-4

Final Report, July 1981

Prepared by

LOS ALAMOS SCIENTIFIC LABORATORY
Los Alamos, New Mexico 87545

Principal Investigators
J. R. Phillips
B. K. Barnes
M. L. Barnes
D. K. Hamlin
E. G. Medina-Ortega

Prepared for

Electric Power Research Institute
3412 Hillview Avenue
Palo Alto, California 94304

EPRI Project Manager
H. Ocken

Materials and Corrosion Program
Nuclear Power Division

ORDERING INFORMATION

Requests for copies of this report should be directed to Research Reports Center (RRC), Box 50490, Palo Alto, CA 94303, (415) 965-4081. There is no charge for reports requested by EPRI member utilities and affiliates, contributing nonmembers, U.S. utility associations, U.S. government agencies (federal, state, and local), media, and foreign organizations with which EPRI has an information exchange agreement. On request, RRC will send a catalog of EPRI reports.

NOTICE

Prepared by
Los Alamos Scientific Laboratory
Los Alamos, New Mexico

EPRI PERSPECTIVE

PROJECT DESCRIPTION

This report addresses the potential of two-dimensional gamma scanning as a nondestructive technique to determine the axial and radial distribution of fission products in irradiated LWR fuel rods. Topics discussed include (1) different unfolding techniques that are used to calculate fission product distributions from measured gamma-ray spectra, (2) a brief review of the components that make up a scanning system, (3) analytic results obtained by using different reconstruction methods (unfolding techniques) from a small number of projections, and (4) experimental results obtained from measurements on a fast breeder fuel pin and a LWR fuel rod.

PROJECT OBJECTIVES

This work was supported as part of the core materials subprogram. The primary goal of this subprogram is to reduce nuclear plant capacity factor losses that arise from concerns about fuel rod failures due to pellet-clad interaction. Earlier work reported in EPRI Final Report NP-1557 indicated that the migration and release of fission products from fuel pellets to the inner surface of the Zircaloy cladding is one key step in the process that eventually can result in cladding failure. Therefore, an incentive exists to evaluate nondestructive methods that could provide information as to when the distribution of aggressive fission products at the periphery of the fuel pellet has reached an unacceptable level. Two-dimensional gamma scanning routinely has been used to nondestructively inspect breeder fuel pins. The primary aims in supporting this work were (1) to provide background information about the technique and (2) to assess the feasibility of using this technique to inspect LWR fuel rods.

PROJECT RESULTS

This review suggests that two-dimensional gamma scanning holds potential as a nondestructive method for inspecting LWR fuel rods. Significant support would be required before this technique could be used to inspect LWR fuel rods at either a poolside site or in a hot cell. The design of a given system would depend upon the information desired. Requirements for both hardware and software differ depending

upon whether the primary interest is in learning about deposition of fission products in the pellet-clad gap region or about fission-product migration within the fuel pellets. For the various methods that were used to reconstruct a picture from a small number of projections, the filtered backprojection Fourier transform technique yielded the best reconstruction.

This report should be of interest to utility personnel with interests or responsibilities in nondestructive inspection, core physics, or fuel performance.

Howard Ocken, Project Manager
Nuclear Power Division

ABSTRACT

Reconstruction of the radial two-dimensional distributions of fission products using projections obtained by nondestructive gamma scanning was evaluated. The filtered backprojection algorithm provided the best reconstruction for simulated gamma-ray sources, as well as for actual irradiated fuel material. Both a low-burnup (11.5 GWd/tU) light-water reactor fuel rod and a high-burnup (179.1 GWd/tU) fast breeder reactor fuel rod were examined using this technique.

THIS PAGE

WAS INTENTIONALLY

LEFT BLANK

ACKNOWLEDGMENTS

We wish to thank M. Cannon, G. Minerbo, and K. Hanson for their assistance in providing the computer codes and technical advice. J. N. Quintana and A. S. Murray provided the technical support on the scanning of the fuel sections. Although an extensive literature search was conducted as part of this evaluation, and we have attempted to cite all the appropriate references, there are many additional references that could have been cited.

THIS PAGE

WAS INTENTIONALLY

LEFT BLANK

CONTENTS

THIS PAGE

WAS INTENTIONALLY

LEFT BLANK

ILLUSTRATIONS

THIS PAGE

WAS INTENTIONALLY

LEFT BLANK

TABLES

Section 1

INTRODUCTION AND SUMMARY

Nondestructive measurement techniques are widely accepted as an integral part of any complete fuel characterization program. Precision gamma scanning has been repeatedly demonstrated as the only nondestructive technique capable of quantitatively measuring the axial and radial distributions of fission products in irradiated fuel materials. The specific distributions of fission products can be used to describe accurately the performance of the fuel material.

The use of precision gamma scanning to measure the axial distribution of fission products has been described by many investigators (1,2). The radial isotopic distributions of fission products have usually been measured by sectioning the fuel rod and performing subsequent analyses by gamma scanning or electron microprobe. A technique was developed at Los Alamos National Laboratory to obtain nondestructively the two-dimensional distribution of fission products at specific axial positions by measuring diametral scans at two or more angular orientations and unfolding these projections (3,4). This nondestructive technique has been applied for the past ten years in the postirradiation examination of experimental fuel materials.

This type of unfolding technique can be applied to the examination of light-water reactor (LWR) fuels at either a hot-cell facility or at the reactor spent-fuel storage basin. To demonstrate the applicability of this type of technique, both low-burnup LWR and high-burnup fast-breeder reactor (FBR) fuel specimens were measured. We have included a discussion of various unfolding techniques and the effects of counting statistics and slit sizes on the reconstructed images, and have identified areas where further refinements may be possible. The filtered backprojection reconstruction technique appears to provide the best representation of the radial distribution of fission products within actual fuel rods for the reconstruction techniques we have evaluated.

This report is basically divided into four sections, followed by four appendices. The first section discusses the theoretical background of

reconstruction and several of the techniques evaluated during this investigation. The second section presents the components of the scanning system. The third section shows results of using filtered backprojection on test cases and irradiated fuel materials. The fourth section presents some of the problems that must be considered in any implementation. A series of appendices covers the effects of statistical uncertainties and slit collimation and compares four reconstruction techniques. The conclusion of the work reported here is that it is feasible to adapt this technique for implementation at reactor spent-fuel storage facilities as a routine part of fuel examinations.

Section 2

THEORETICAL BACKGROUND

A. GENERAL

Reconstruction of images from projections has many scientific and medical applications where the invasion or destruction of the object is unacceptable. This noninvasive technique or procedure has been labeled many things: "computed tomography," "computerized axial tomography," "transaxial tomography," and "reconstruction from projections." Regardless of the varying names of the techniques, the procedure is that of mathematically combining projections from radiation emissions or transmissions at various angles to obtain an accurate representation of the original object.

The first work in the reconstruction of an object possessing circular symmetry from projections was published in 1826 by Abel (5). The groundwork for the present-day procedures was laid in 1917 by the Austrian mathematician Radon (6), who solved the basic mathematics of the problem. Radon's significant contribution was a set of integral equations that related two-dimensional, non-symmetric objects to their projections. He mathematically proved that a two- or three-dimensional object can be uniquely reconstructed from an infinite set of its projections. These formulas have served as the basis of the theoretical and practical development of the reconstruction technique. Mathematicians, image analysts, radio astronomers, and medical radiologists have repeatedly rediscovered and made modifications of Radon's classical inversion formula. However, the application of reconstruction techniques has been tied to the development of computer technology because of the tremendous number of computations involved.

The input data for all of these techniques are projections obtained at two or more angular orientations. In Fig. 2-1 the function $g(x,y)$ represents the distribution of the physical property of interest -- in our particular case, the radial distribution of a fission product. The projection data are estimates of the line integral of the function $g(x,y)$, where the line of integration is specified by the parameters s and θ. The s,t axes are rotated by an angle θ from

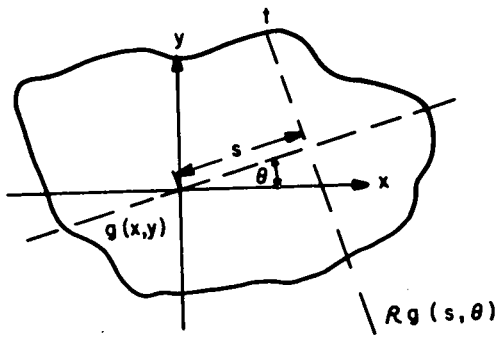

Figure 2-1. Each projection is an estimate of the line integral of the function g(x,y), where the line of integration is specified by the parameters s and θ. Geometrical relation between a two-dimensional source g(x,y) and the measured projection $\mathcal{R}g(s,\theta)$.

the x,y axes. Then, the line integral of g along the line specified by (s,θ) can be denoted by $[\mathcal{R}g](s,\theta)$, where $\mathcal{R}$ is the Radon operator (named in honor of Radon). The function $\mathcal{R}g$ is obtained by a line integral along t as

$$[\mathcal{R}g](s,\theta) = \int_{-\infty}^{\infty} g(s \cdot \cos\theta - t \cdot \sin\theta,\ s \cdot \sin\theta + t \cdot \cos\theta)dt \ . \quad (1)$$

Radon was the first to study this transformation that maps a function g into a function $\mathcal{R}g$, and subsequently, the inverse transformations to compute g from $\mathcal{R}g$ (7,8).

The reconstruction of images from projections is based on the development of techniques for solving variations of the above integral equation. No single technique has been found capable of satisfactorily processing the wide variety of projection-measurement geometries and the quantity and precision of data that occur in practical applications.

In the measurements of isotopic distributions of fission products in LWR fuel pins, the data may be considered to be projection measurements or sets of line integrals of gamma-ray emission at specified intervals across the pin.

B. ALGORITHMS

The problem of reconstruction is essentially: "Given a subset of all possible projections of an object, estimate its internal density distribution. All algorithms for reconstruction take as input the projection data, and all produce as output an estimate of the original structure based on the available data. The estimate varies from method to method. The relative performance of the various methods depends on the object and how the data are collected." (9)

All of the reconstruction techniques are limited because they can only provide an estimate of the internal density distribution. Mathematical reconstruction from a finite set of projection data is known to be an indeterminate problem (10,11). A very large number of algorithms exists for reconstructing objects from their projections. It would be useful to have some guidelines to determine which algorithms are most appropriate under specific circumstances. Unfortunately, little has been published in this direction.

Several criteria must be kept in mind when selecting a reconstruction algorithm. First and most important is the requirement that the reconstruction be consistent with the data available to the algorithm (artifacts are not introduced). This means that the projections (ray-sum) of the reconstructed picture should be the same as the ray-sum of the original distribution. With a finite number of projections, an approximation is the best result that can be attained (9).

Secondly, a simple way must be available of deciding whether the reconstruction algorithm has successfully approximated the original distribution. A third factor involves the cost (manpower and financial) of applying a specific reconstruction algorithm. In actual applications, a large number of reconstructions and interpolations are involved and these may be cost prohibitive.

There are two ways of comparing reconstruction algorithms: theoretical and experimental. A theoretical comparison can be either a mathematical or a purely descriptive discussion of the nature of the methods under consideration (for example, method A is better than method B because it has a certain desirable property). The experimental method of comparison consists either of constructing test objects (phantoms) and physically taking their projections, or of designing test patterns and working out their projections mathematically; in either case, the various algorithms are used on the projection data, and the reconstructions are then compared to the original distribution (9).

An exhaustive experimental comparison between algorithms must span the following combinations of factors:

1. A diversity of test patterns representative of all possible cases of interest.
2. A diversity of modes of taking projections. This includes, for example:
   a. variation in the number of projections to obtain both well-determined and highly underdetermined cases
   b. variation in the range of angles of the projections
   c. both parallel and divergent rays and overlapping rays defined by partial collimators, as in nuclear medicine.
3. Variation in the range of angles of the projections.
4. Errors due to mechanical problems, such as accuracy in measuring the angles and spacings of the projections; and location of a common origin for the projections, motion, or degradation of the object being examined.
5. Variation in the fineness of digitization or the number of basis functions to be used.

No reconstruction algorithm has been tested for all combinations of these factors, nor has any been compared to another using them. The combinations of factors involved in such a comparision are overwhelming, especially considering the large number of algorithms. Thus, all experimental comparative studies to date must be taken as more or less inadequate. However, Budinger and Gullberg (12) have reviewed the status of three-dimensional reconstruction by iterative least-squares and Fourier transform techniques.

Most of these factors have not been studied from a theoretical viewpoint. As Herman and Rowland pointed out (13), theoretical comparisons are difficult because there is no common mathematical foundation for the reconstruction algorithms (without gross oversimplifications). Moreover, the most we could hope for would be an estimate of average- or worst-case performance. Since a given application usually concentrates on one type of picture, for which one algorithm may excel, general theoretical pronouncements may be of little value. For these reasons we have concentrated on experimental comparisons.

1. Backprojection

The most common reconstruction algorithm includes an operation referred to as backprojection, based on the previously described work of Radon (6). Fundamental to understanding reconstruction from projection is the central-slice, or projection-slice, theorem. This theorem states "that a one-dimensional Fourier

transform of a one-dimensional projection of a two-dimensional object is mathematically identical to one line (a slice) through the two-dimensional Fourier transform of the object itself. Thus, knowledge of all one-dimensional projections is sufficient to synthesize the two-dimensional transform of the object from which the object is readily obtained by an inverse two-dimensional transform."(14)

The quality of the projection images can be improved by using appropriate correcting functions. Correcting in the Fourier spaces is done by taking the Fourier transform of the degraded image, multiplying the transform by a correcting filter function, and performing the inverse Fourier transform. The filter we used performed a ramp function that tended to filter out high-frequency noise.

The Fourier method depends on transforming the projections into Fourier space, where they define part of the Fourier transform of the whole object. Each projection may be shown to yield values on a central section of Fourier space, which is a line or plane (corresponding to the two- or three-dimensional problem) through the origin at an angle corresponding to the direction of the projection in real space. An attempt is then made to interpolate the unknown values of the full Fourier transform from the values on the central sections. After interpolation a reverse Fourier transform provides an estimate of the object's structure.

2. Iterative Techniques

Iterative techniques are the basis of another set of algorithms used in the reconstruction of distributions from projections. One iterative technique is the algebraic reconstruction technique (ART). It can be called a "direct technique" because the reconstruction is done entirely in the density or real space without using Fourier transforms.

As the number of projections increase, ART results gradually improve. In Herman (15), eight projections seems to be a "critical" number with five iterations producing "superior" results. It should be emphasized that one can only hope to obtain a reasonable representation, since it has been proved that a nontrivial picture cannot be uniquely determined from a finite number of projections (9).

Gordon explains the basic idea behind ART: "Starting from a blank picture, the ray-sums of all the projections are satisfied one after the other by distributing the difference between the desired ray-sum and the actual ray-sum equally among all the points in the ray. While satisfying the ray-sums of a particular projection, the process usually disturbs the ray-sums of previously satisfied projections. However, as we repeatedly go through satisfying all the projections, the disturbances get smaller and smaller, and eventually the method converges to a picture which satisfies all projections."(15)

Because changes are made fairly uniformly, the final product is the smoothest reconstruction satisfying the given projections. In general, the reconstructed image shows only those features that are forced on it by the projections and not those features introduced by the reconstruction process.

One iteration is considered to be the process of satisfying all projections one after the other only once. Predictably, accuracy of ART increases with the number of iterations. At first, the successive pictures become progressively better, but once an "optimum stopping point" is passed, the reconstructions become progressively worse. This phenomenon has been further examined by Herman et al (16). One must remember that the "ideal outcome cannot be attained due to limitations on the amount and quality of data as well as the reconstruction algorithms themselves."(17)

Iterative methods may differ in the way the corrections are calculated and reapplied during each iteration. In Gordon's tutorial on ART (17) he states that the choice between additive ART and multiplicative ART (MART) depends on the physics of the radiation used. "For transmitted radiation, the form of the reconstructed object should be independent of an additive constant. Such a constant may result from variable exposure in an x-ray, variable development of the film, or an intervening filter...."

In studies by Minerbo and Sanderson (18), and Gordon, Bender, and Herman (19), MART reconstruction was claimed to be able to produce a solution with the largest maximum entropy. As early as 1971, Gordon, Bender, and Herman were trying to develop reconstruction algorithms that would give solutions that were minimally biased because of maximized entropy. It has been noted (19) but not proved for the general case that since the entropy of the source function increases with iteration when the multiplicative ART algorithm is used, there is a relation between MART and the maximum entropy solution.

One iterative algorithm, maximum entropy (MENT), has been implemented to produce a maximum entropy solution to the problem of reconstructing a source from a discrete set of projections (20). In general, maximum entropy techniques are powerful but expensive with respect to computing time. From the standpoint of information theory, the maximum entropy technique is conceptually attractive. It yields the image with the lowest information content consistent with the available data. Thus with this approach one avoids introducing extraneous information or artificial structures. The problem of reconstructing a source distribution from a limited number of projections is known to be indeterminate. "A maximum entropy method thus seems attractive for this problem, especially when the available projection data are incomplete or degraded by noise errors"(20). By being an indeterminate problem, it is implied that an infinite number of non-unique solutions can satisfy the limiting criteria imposed on the solution by the actual data. When the data source has a simple structure or is close to circular symmetry in shape, one can use this a priori knowledge to eliminate various "unacceptable" results.

MENT may be considered an iterative technique for solving a constrained optimization problem. A constraint approach enhances a desired feature of the data at the expense of blurring other parts. The maximum entropy approach will not introduce new information but may not reproduce all "real" information either (20).

Minerbo has shown (20) that with a small number of views (<10) iterative methods generally perform better than either Fourier space inversions or convolutional backprojection methods. MENT was originally developed to provide a maximum entropy solution that would not exhibit some of the "streaking" artifacts of ART and MART, which occur with a small number of projections.

3. Geometrical Unfolding

The original unfolding technique developed at Los Alamos, Two-dimensional (TWODIM) (3,4), involved the computation of the source intensity of successive rings that were defined by the stepsize of the diametral scans or projections. This successive solution of each ring has the tendency to be highly dependent on the noise of the projection data. A subsequent modification of the technique eliminated this instability problem but decreased the resolution of the technique. This effect is clearly demonstrated in Appendix D.

4. Summary of Algorithms

We have evaluated the applicability of four techniques: backprojection, MART, MENT, and TWODIM, for reconstructing projections of a fission product to obtain the best estimate of its two-dimensional distribution. The backprojection technique appeared to be superior for all of our test cases, as well as for the two fuel specimens examined. Therefore, the backprojection technique will be used in the remainder of the report as the preferred technique. For a detailed comparison of the four techniques, refer to Appendix D.

Section 3

SCANNING SYSTEM COMPONENTS

The precision gamma scanning system used in the measurements essentially consisted of four separate components: (a) a scanning mechanism for the precise positioning of the irradiated fuel rod, (b) collimators for the precise definition of the volume segment from which the gamma-ray spectra were collected, (c) a high-resolution detector assembly, and (d) an automated data acquisition unit (Fig. 3-1).

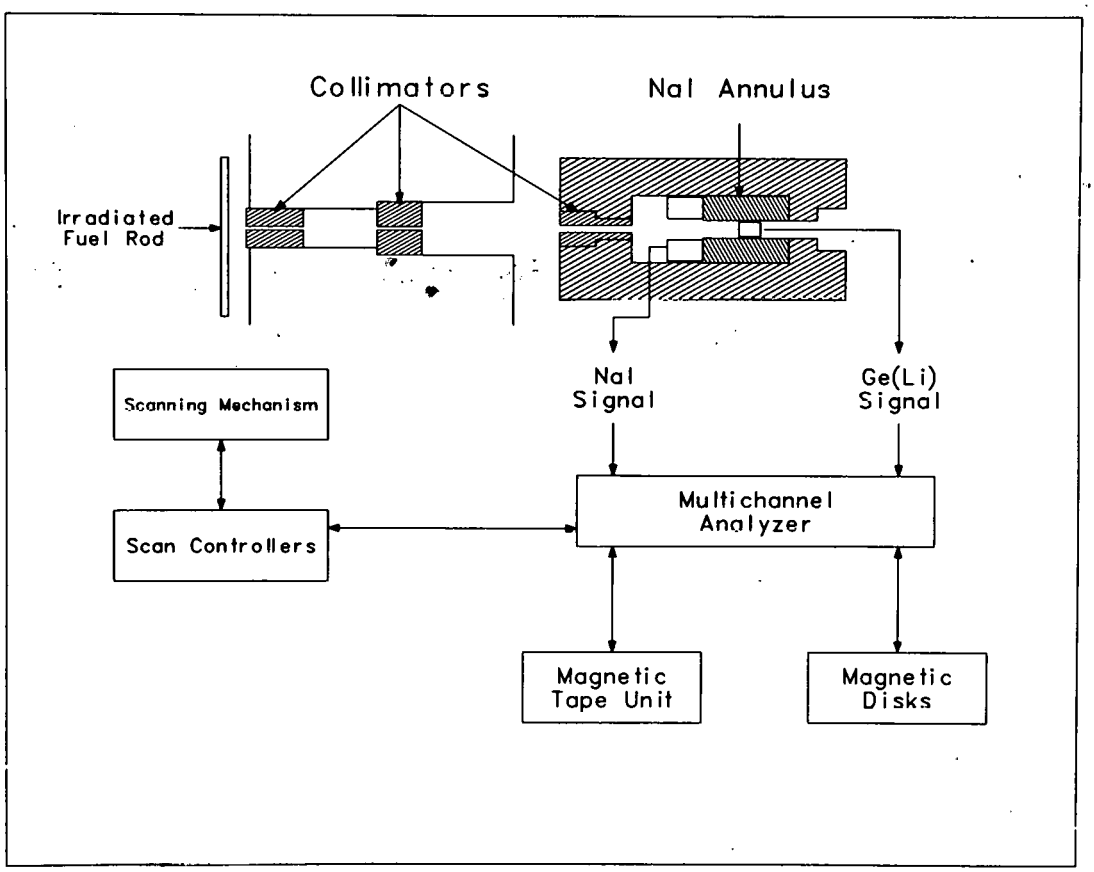

Figure 3-1. Schematic of scanning system used in this investigation.

A. SCANNING MECHANISM

The scanning mechanism shown in Fig. 3-2 had five degrees of movement: x, y, z, tilt, and rotation. Each motion was controlled by precision stepping motors coupled to absolute position shaft encoders with binary-coded-decimal (BCD) readouts. The individual degrees of movement: x, y, z, and tilt, were positioned with a precision of 0.0025 cm (±0.001 in.), and the rotation motion was set with a precision of ±1.8°. The scanning mechanism accommodated fuel pins 60 to 160 cm (24 to 63 in.) long and up to 7.5 cm in diameter.

The accuracy of the x, y, and z motions were: x (horizontal), ±0.00127 cm (±0.0005 in.) over 15.0 cm (6.0 in.); y, ±0.0051 cm (±0.002 in.) over 80 cm (32.0 in.); and z (vertical), ±0.0051 cm (±0.002 in.) over 160 cm (63 in.) of travel. The precision ball screws had a 0.508-cm (0.200-in.) pitch resulting in five

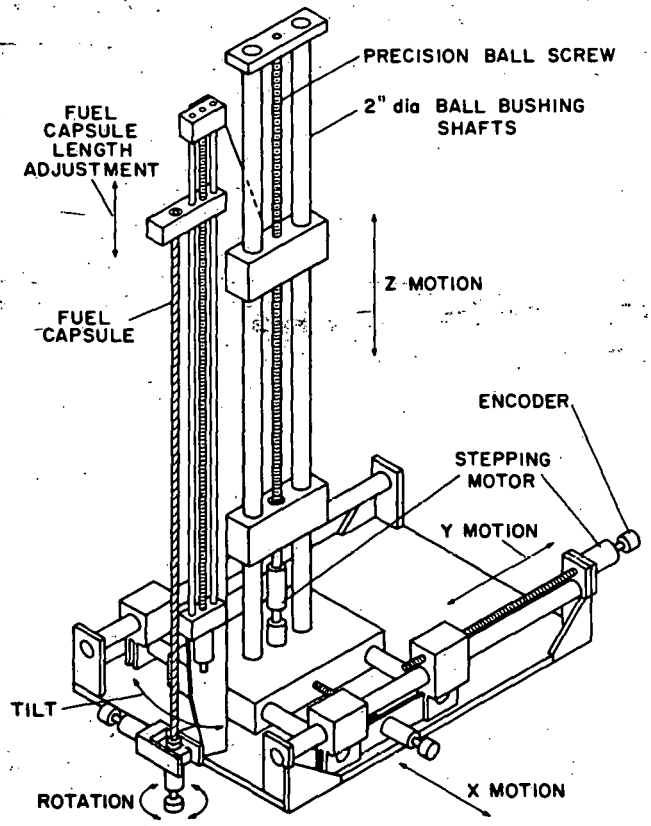

Figure 3-2. Scanning mechanism for positioning irradiated fuel rods.

resolutions per inch of travel. The ball screws were attached to Slo-Syn precision stepping motors having 200 steps per revolution. The absolute position of each motion was obtained from bidirectional position shaft encoders with a BCD readout from 0.0 to 254.000 cm (0.0 to 99.999 in.). The shaft encoder and the bifilar stepping motors had 200 divisions per revolution and therefore were attached to the stepping motor shafts. Because of space limitations in the hot cell, the z (vertical)-shaft encoder was attached directly to the stepping motor shaft, and the x, y, tilt, and rotation encoders were coupled to their motors through spring-loaded anti-backlash gears.

The scanning mechanism was designed without any structural material in line with the collimating slit and the fuel pin. This design reduced the occurrence of backscatter peaks from the Compton scattering that might have interfered with or been mistaken for the full-energy peaks. The scanning mechanism was placed in a 180 x 180 cm (6 x 6 ft.) hot cell with 88-cm (34.75-in.)-thick walls that allowed the examination of irradiated fuel pins with up to 10 kCi of 1 MeV gamma rays (Fig. 3-3).

A similar scanning mechanism can be designed for handling LWR fuel rods in a hot cell facility. The most critical factor to be considered is the precision of the horizontal motion because it will limit the spatial resolution of the technique. The scanning mechanism described above had very rigid restrictions placed on all the positioning components; these restrictions would probably not be essential except for the restriction on the horizontal motion.

B. COLLIMATORS

Precise collimation of the gamma-ray beam is required to obtain the spatial distributions of the gamma-ray emitting isotopes. In this particular investigation, we used a collimator arrangement consisting of three separate collimators: a primary collimator, which precisely defined the volume segment of the fuel rod, and two beam scraping collimators that shielded the anticoincidence annulus from the gamma-ray beam.

Selection of the size of collimator to use for examination of a specific fuel rod depends on the spatial resolution desired and the activity of the fuel material. For example, the fraction of gamma rays originating in the volume segment of a typical LWR fuel rod defined by the collimating slits that strike the surface of the detector was about 2.2×10^{-8} for gamma rays with energies of 600 keV. In

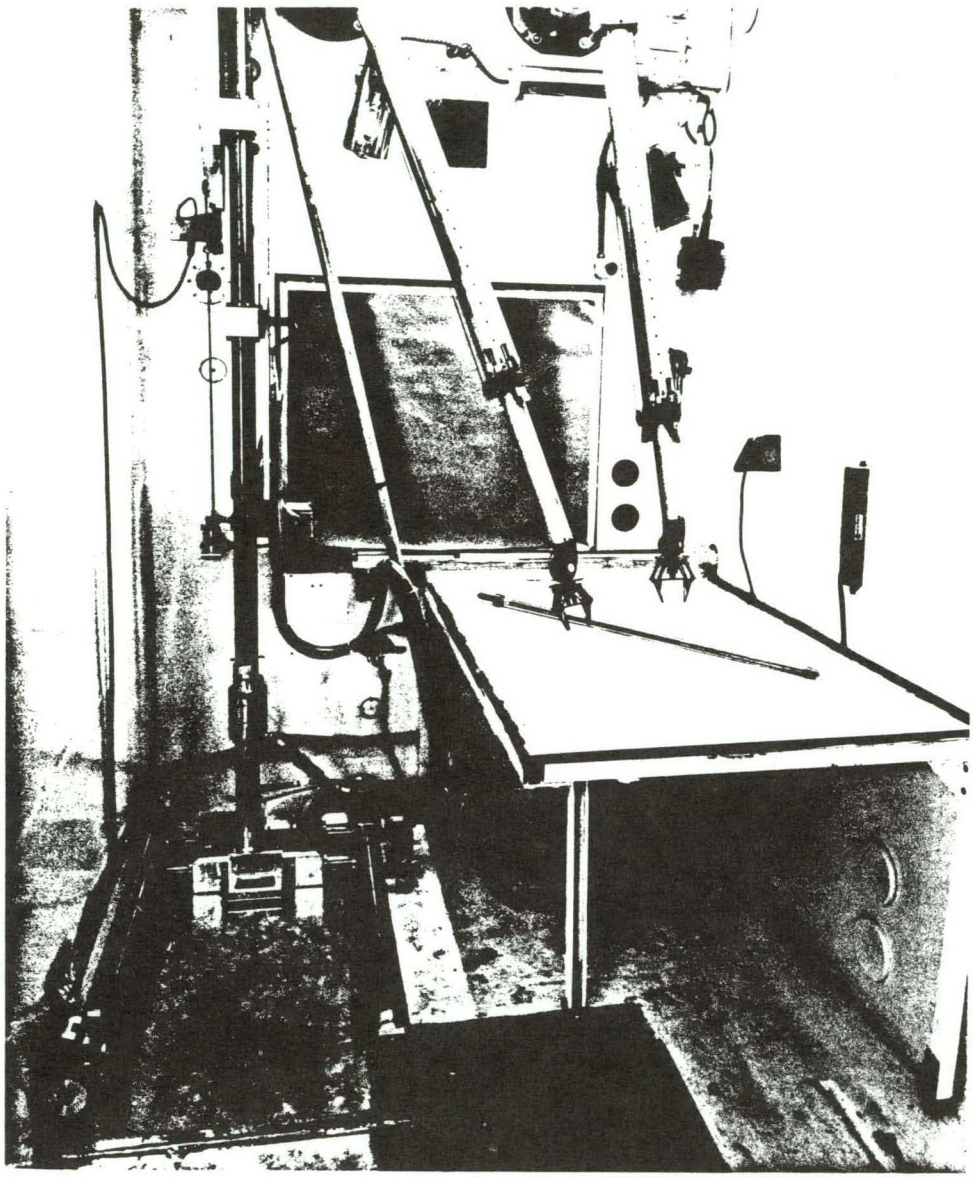

Figure 3-3. Scanning mechanism installed in hot cell.

typical LWR fuel with exposures of about 30 GWd/tU, there are 45 x 10^{18} ^{137}Cs atoms/cm^3. Incorporating the fraction above for a fuel volume of 0.023 cm^3 (maximum fuel volume viewed by our system) and the branching ratio of the 661.6-keV gamma ray of ^{137}Cs (0.851), only 850 gamma rays will strike the surface of the detector per minute. If a detector with 15 percent efficiency for this energy were used, it would require at least 10 minutes to obtain 1000 counts in the full-energy peak, which may have approximately a 5 percent error associated with it depending upon the background from higher energy gamma rays.

This discussion may be somewhat involved, but it is essential for understanding how critical the selection of the collimators is in obtaining meaningful results within reasonable examination periods. Both source activity levels and spatial resolution requirements must be considered in the design of any gamma scanning system.

C. DETECTOR ASSEMBLY

The detector assembly consisted of a large, high-resolution Ge(Li) detector surrounded by a 20 x 30 cm NaI (Tl) anticoincidence annulus encased in a low gamma activity lead cask. This detector assembly produced very high-quality gamma-ray spectra with peak-to-Compton ratios greater than 100. Present day detectors can give peak-to-Compton ratios of at least 30 to 1 and are more than adequate for measuring LWR spent fuel. Lead shielding is required to reduce the background, with 5 cm of lead being more than adequate.

D. DATA ACQUISITION UNIT

The data acquisition unit was automated to control the scanning mechanism as well as to collect and analyze gamma-ray spectra (21). The unit positions the fuel rod, collects the gamma-ray spectra, then automatically moves the fuel rod to the next position. Similar data acquisition systems are readily available from private industry.

The processing of the two-dimensional data was not performed on the data acquisition unit, but rather on larger computers that had enhanced graphics capabilities. The data processing techniques used in the generation of the two-dimensional distribution could be implemented on a minicomputer.

E. COMPONENT SUMMARY

Each of the four components of the gamma scanning system has been discussed in the previous sections. Most of the discussion has been centered on the design of the scanning mechanism and the collimators because they are the most critical components. Detectors and data acquisition units are available from a wide variety of vendors and can be modified as necessary. However, if the scanning mechanisms or collimators are not designed appropriately, the system may never function correctly.

The next section discusses various unfolding algorithms that may be applied to the data obtained using the scanning systems. None of these algorithms can compensate for data obtained from a poorly designed scanning system.

Section 4

RESULTS

A. SIMULATED TEST CASE

Four techniques to reconstruct a picture from a small number of projections have been compared experimentally: a filtered backprojection Fourier transform technique (TOMO) (12,22), a multiplicative algebraic iterative reconstruction technique (MART) (23), and finally, a recent adaptation of the algebraic reconstruction technique (ART) algorithm to a maximum entropy (MENT) criterion (20,24), and the TWODIM unfolding algorithm (3,4).

The data used for comparision of these techniques were projections generated by a computer program (TWOCHK) described in Appendix A. This program analytically simulates projections at specified angular orientations of various distribution functions. This code was used to generate the set of test data discussed in Appendices A through D. A typical example of the type of test data generated is presented in Fig. 4-1, in which a narrow ring was superimposed on a uniform source. This distribution is similar to the distribution of a volatile isotope that migrates radially to the pellet-cladding interface (for example, cesium and iodine isotopes). The entire source was skewed over the simulated scan region to reflect a 30 percent change across the diameter of the fuel rod. The data were constructed to cover a 1.27- x 1.27-cm area in 0.0127-cm steps (101 x 101 matrix). Six projections were calculated at 30° intervals from 0° to 150° (Fig. 4-2). The six resulting projections were the test input data for the reconstruction algorithms.

The filtered backprojection Fourier transform technique resulted in the best reconstruction. A comparison of all four reconstruction techniques is presented in Appendix D. The computer code TOMO is, by nature of the backprojection algorithm, best suited for a large number of projections. When only a few projections are used in the algorithm, the reconstruction is very poor.

A much more realistic-appearing reconstruction can be obtained from the backprojection algorithm, however, by providing a larger number of projections.

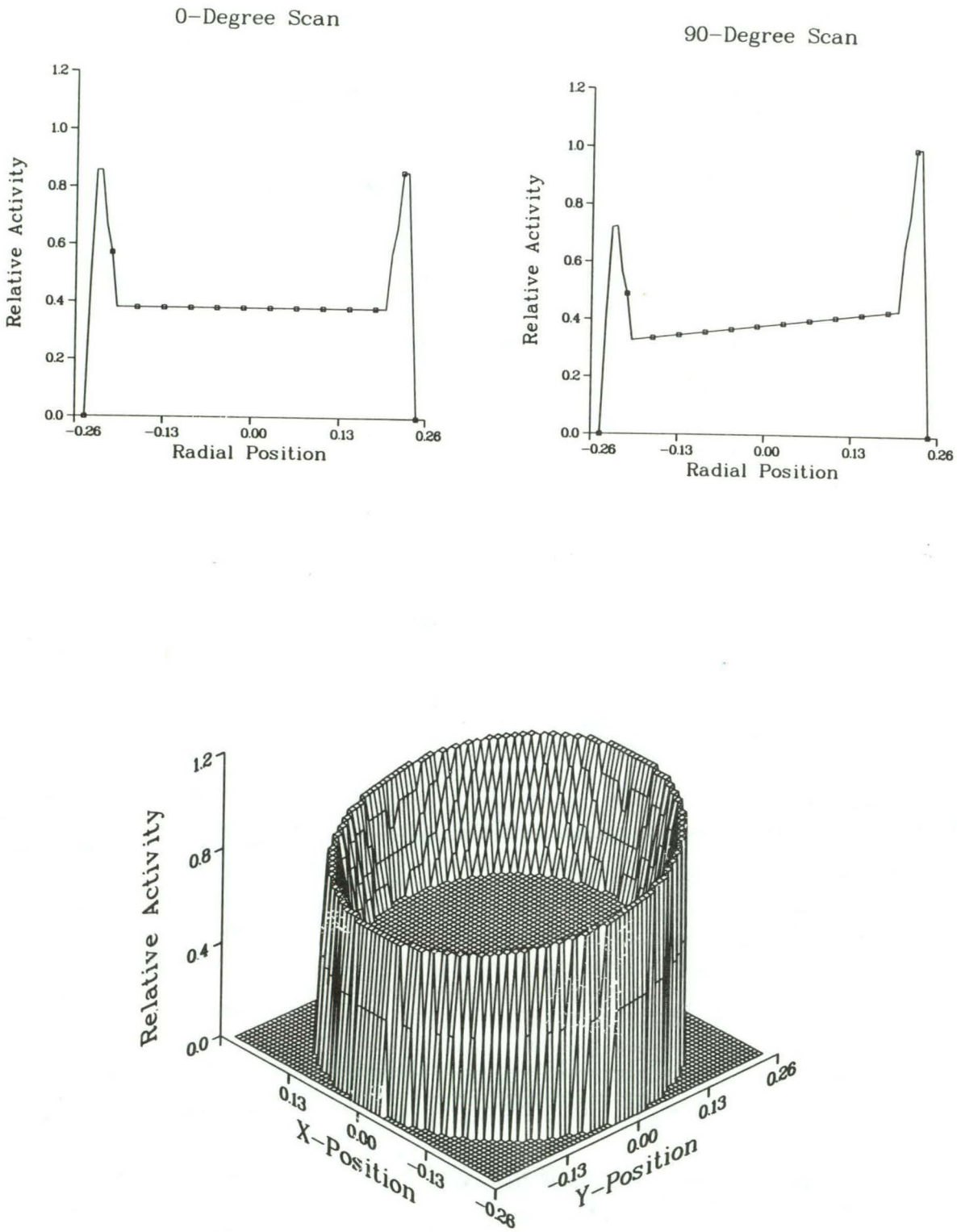

Figure 4-1. Radial scans across the diameter of the simulated gamma-ray source and isometric projection of the density distribution matrix.

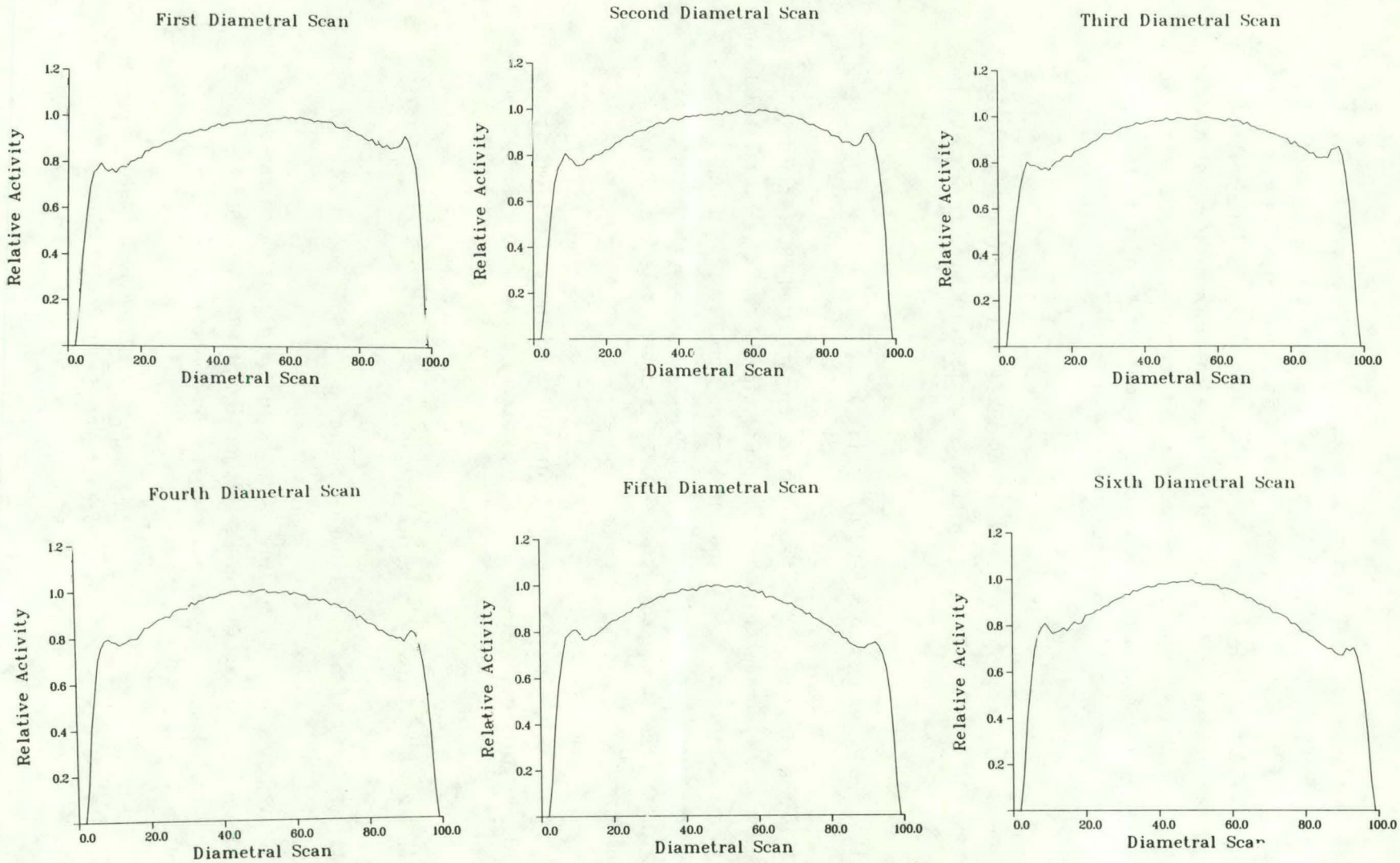

Figure 4-2. Set of six diametral projections at 30° intervals for the simulated gamma-ray source.

Ideally, if time permits, real measured projections would be preferred. However, if only two projections (or some small number) are measured, the visual appearance of the reconstruction can be greatly improved by an interpolation scheme that provides a large number of calculated projections interpolated from the measured projections. This does not increase the information content of the reconstruction, but does produce a reconstruction more consistent with the known circular shape of the fuel pin. The concept is somewhat similar to that of smoothing data to improve its appearance even when information is actually lost in the process.

The projections (2, 4, or 6) have been interpolated to 181 projections in the 0°-180° range at 1° intervals. The calculated projections were created by the interpolation formula

$$PROJ(I) = PROJ(A) * \cos^2 \theta + PROJ(B) * \sin^2 \theta \qquad (2)$$

in which I is the index of the projection that lies between PROJ(A) and PROJ(B). The change of angular orientation between projections A and B is normalized to be equivalent to $\pi/2$ radians. Cos θ and sin θ range from 0.0 to 1.0 and 1.0 to 0.0 in the angular change from projection A to projection B, and since $\cos^2 \theta + \sin^2 \theta = 1.0$, the resulting projection PROJ(I) is appropriately a mixture of projections A and B.

An example of the weighting function for interpolating two projections is shown in Fig. 4-3. In this case, there are only two scans taken at 0° and 90° (scans A and B).

$$PROJ(I) = PROJ(A) * \cos^2 \phi + PROJ(B) * \sin^2 \phi \qquad 0 \leq \phi < 90°, \qquad (3)$$

and

$$PROJ(I) = PROJ(B) * \cos^2 \phi + PROJ(-A) * \sin^2 \phi \qquad 90 < \phi \leq 180°, \qquad (4)$$

where ϕ is equal to 2 θ. The angle θ is the actual angle at which the projection is measured and PROJ(-A) is the reverse projection of PROJ(A). Other possible interpolation techniques were not investigated in the study.

In Fig. 4-4, the results using the filtered backprojection technique are presented. The reconstruction does estimate the original distribution. The 0° radial scan is symmetrical within the precision of the data and the 90° radial

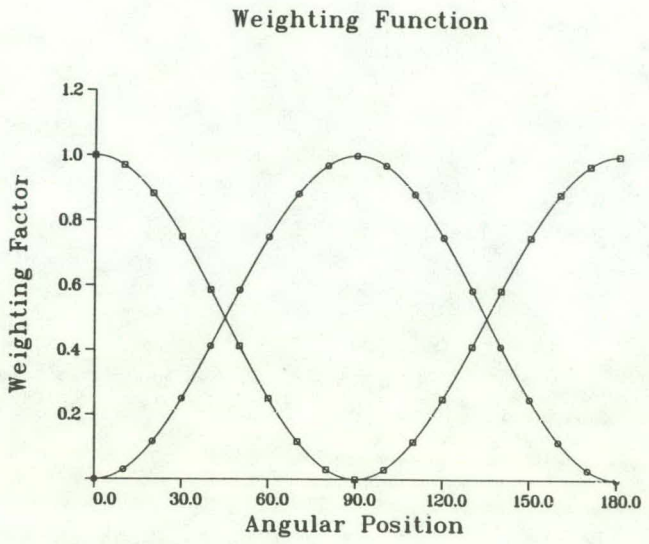

Figure 4-3. Interpolation function used to generate additional projections.

scan does show a skewness similar to the original data. However, the left-hand side of the 90° radial scan should have been at a calculated value of 0.73 and not at the measured value of 0.87. The backprojection algorithm underestimated the skewness, but it estimated the value for the 0° radial scan as 0.88, compared with the true value of 0.87. Considering that this projection was obtained from only six projections, the agreement between the reconstructed image and the original image was very good.

B. LOW-BURNUP BWR FUEL ROD

A low-burnup BWR fuel rod (25) was analyzed using the backprojection reconstruction technique. Table I lists the initial fuel parameters and irradiation history information. The projection data was obtained using a precision scanning mechanism and detector system at the Los Alamos hot cell facility (4). Since the fuel rod had been removed from the reactor for over four years and had a low level of burnup, only the ^{137}Cs isotopic distribution was measured at two angular orientations. The statistical uncertainties of the other isotopes precluded their use except for possibly the ^{134}Cs isotopic distribution that was similar to the ^{137}Cs distribution.

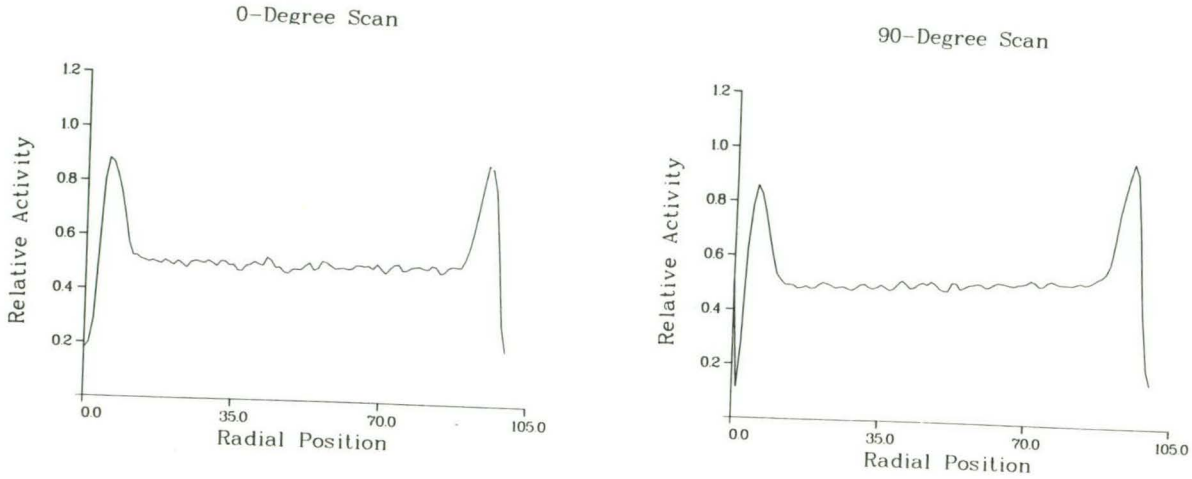

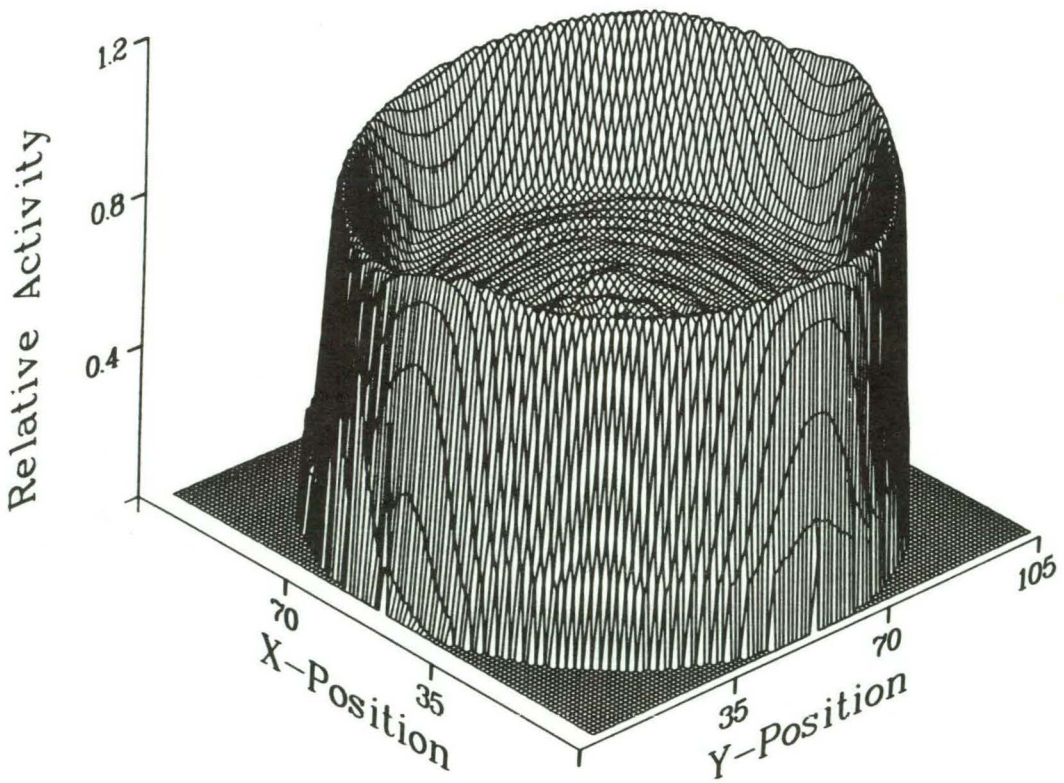

Figure 4-4. Reconstruction of the test case using the filtered backprojection technique.

The two diametral projections are shown in Fig. 4-5. The first diametral scan is rather symmetrical as compared with the second diametral scan that indicates a slightly skewed distribution. It should be stressed that by examining the diametral scans, the experimenter can intuitively determine what the original distribution should be. In Fig. 4-6, the results without any attenuation correction are presented to illustrate the significant influence that the attenuation correction has on the reconstruction. The interpretation of Fig. 9 would imply that the radial ^{137}Cs fission product distribution was distorted toward the outer surface of the fuel pin.

Attenuation corrections significantly alter the results, as can be seen in Fig. 4-7. Only about 60 percent of the 661.6-keV gamma rays of ^{137}Cs escape the surface of the fuel pellet at the center line of the projection; therefore, the attenuation correction procedure exaggerates the structure of the radial scans, particularly in the interior region. This is evident when the 0° scans are compared for the unattenuated results and the attenuated results.

TABLE I

FUEL PARAMETERS AND IRRADIATION HISTORY OF BWR FUEL ROD

Fuel Rod Parameters

Initial ^{235}U enrichment	2.56 wt percent
Stack density	10.32 g/cm^3
Pellet diameter	1.237 cm (0.487 in.)
Cladding	
Material	Zr-2
Thickness	0.094 cm (0.037 in.)
Outside diameter	1.430 cm (0.563 in.)

Irradiation History

7- by 7-fuel assembly geometry
Part of an experimental test assembly that contained MO_2 and UO_2 rods
One cycle exposure - July 1974 to January 1976
Declared burnup - 11,450 MWd/tU

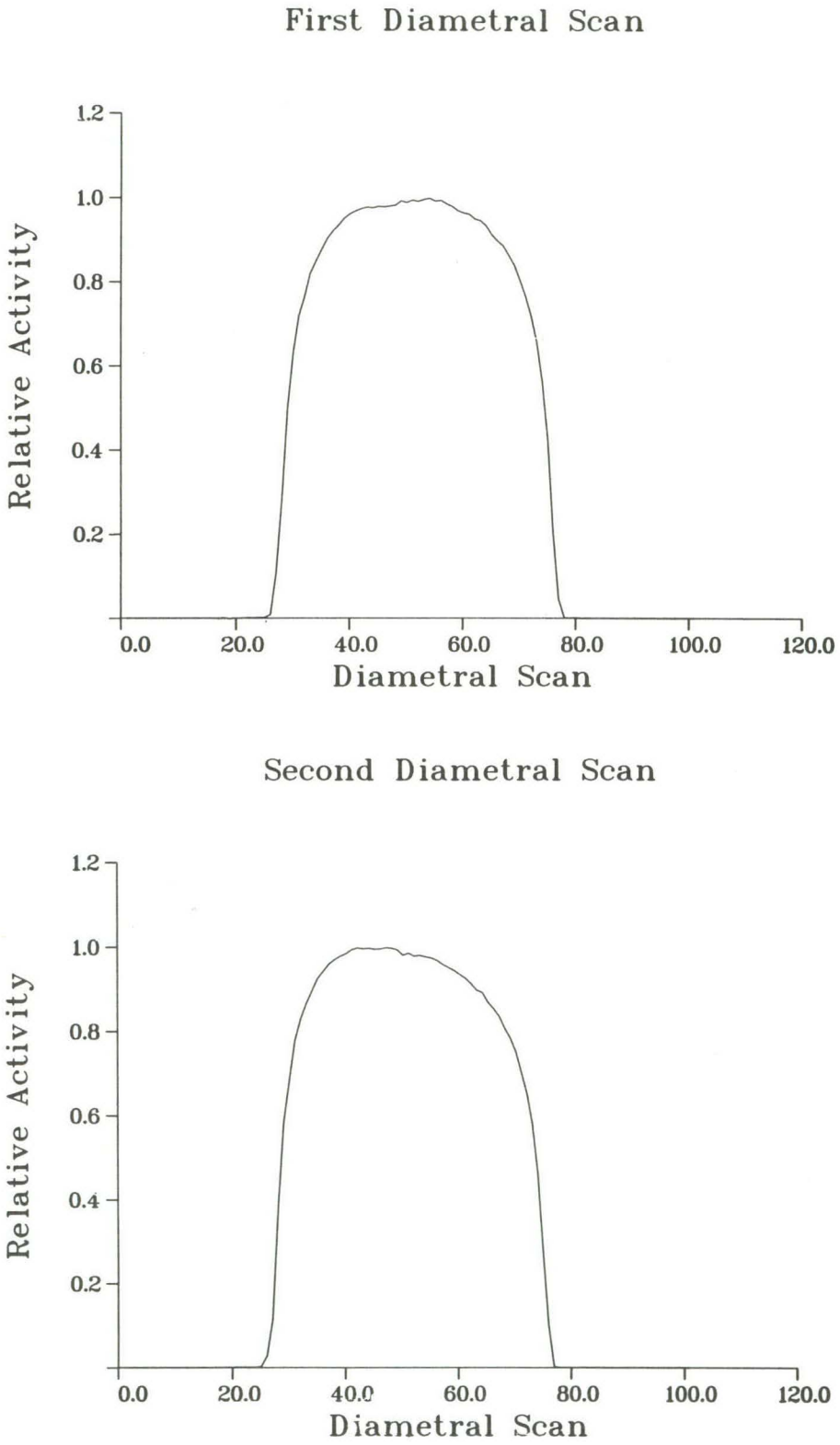

Figure 4-5. Two ^{137}Cs diametral projections for the LWR fuel rod.

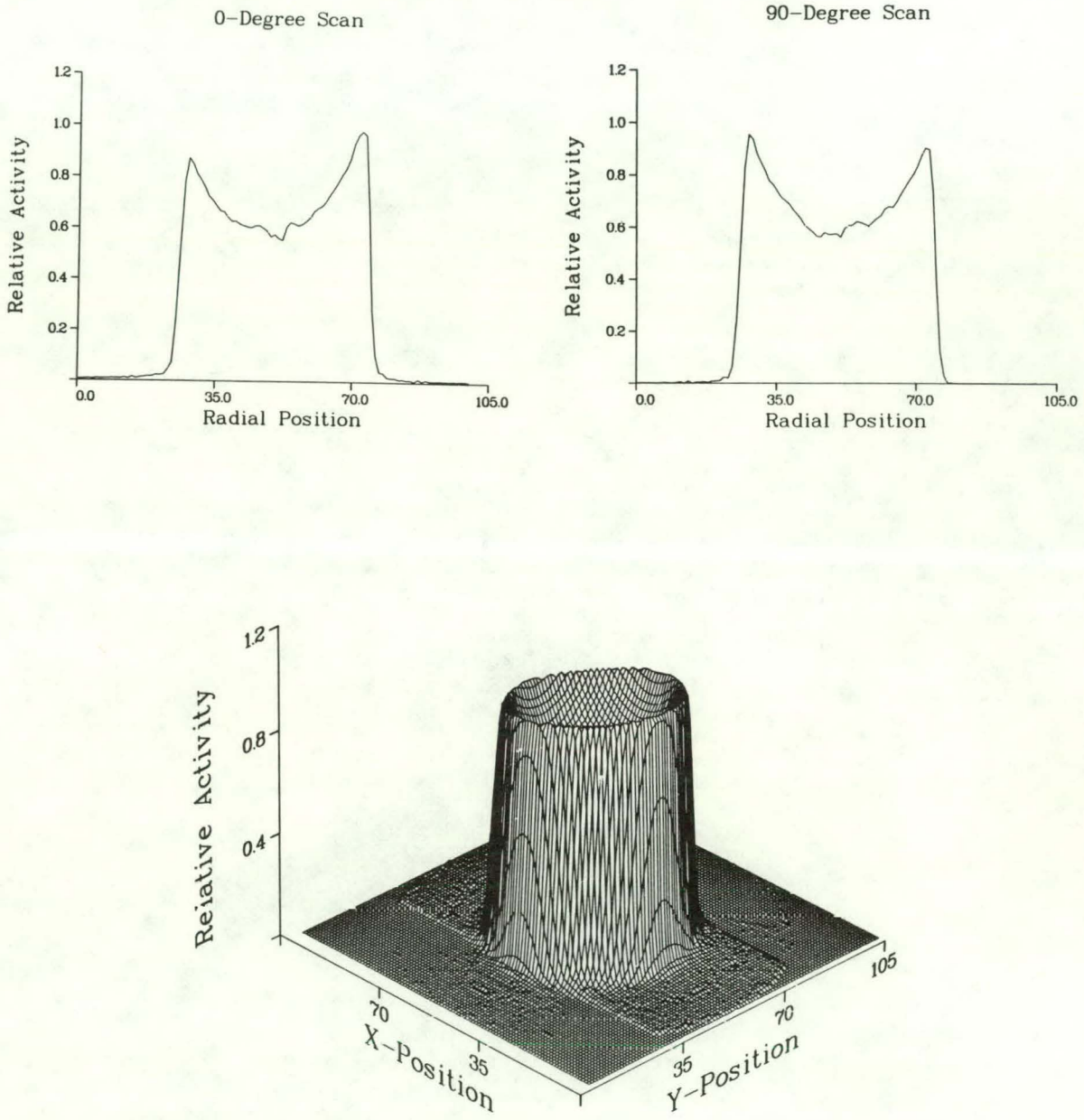

Figure 4-6. Results from backprojection reconstruction without attenuation correction.

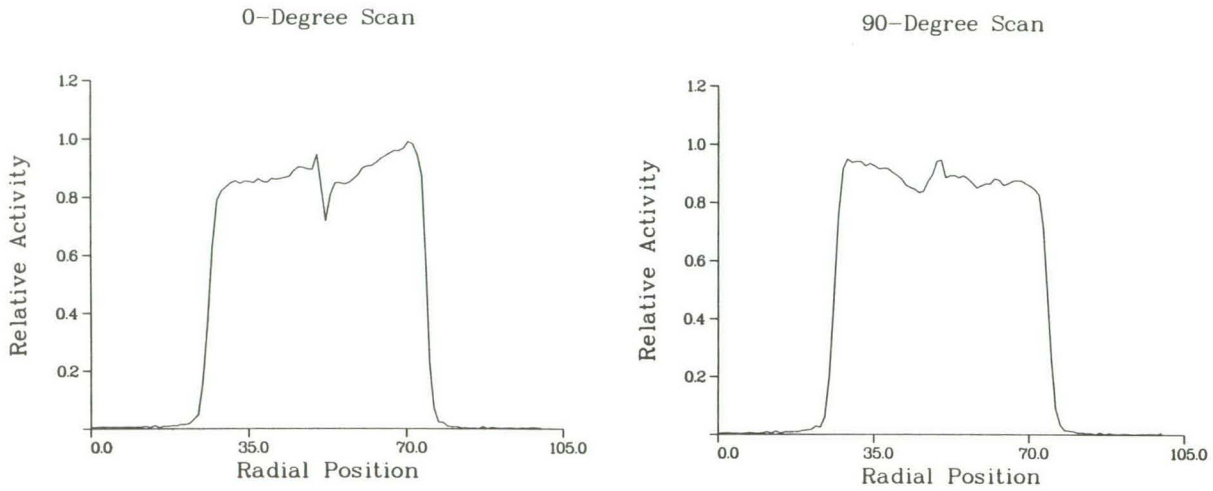

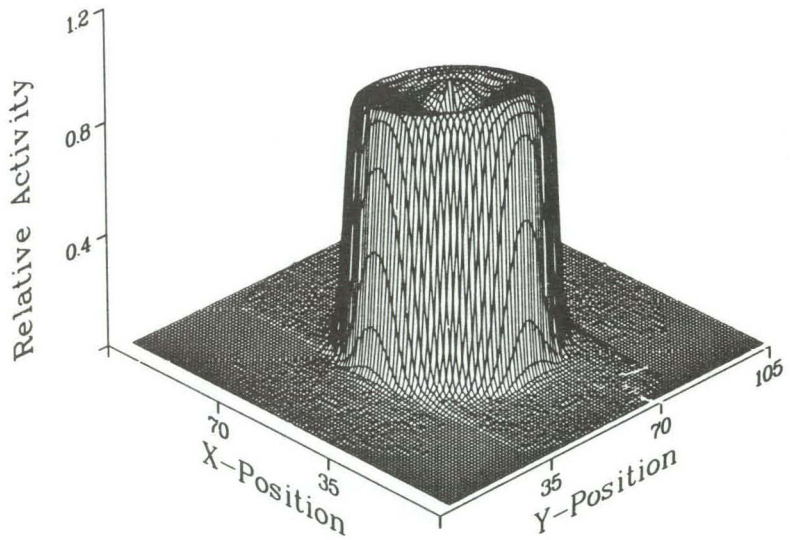

Figure 4-7. Results after the incorporation of the attenuation correction times in the backprojection reconstruction.

C. EXPERIMENTAL FAST BREEDER FUEL ROD

Another fuel section from an experimental assembly was scanned to demonstrate the applicability of using the backprojection reconstruction technique. Only the ^{137}Cs isotopic distribution was measured for the LWR fuel section because of the low burnup and long cooling time. On this FBR fuel section, the two-dimensional isotopic distributions were determined for three fission products (^{137}Cs, ^{134}Cs, and ^{125}Sb) and two cladding activation products (^{54}Mn and ^{60}Co). Table II presents the relevant initial fuel parameters and irradiation history information.

This particular fuel section was scanned at six angular orientations, each separated by 30°, to obtain the input data for the filtered backprojection reconstruction technique. Six projections of the ^{137}Cs isotope are shown in Fig. 4-8. From these projections, it is clear that the isotope is distributed as a ring source, which is confirmed by the calculated results shown in Fig. 4-9. The uncertainty of the input data due to counting statistics was of the

TABLE II

FUEL PARAMETERS AND IRRADIATION HISTORY OF FBR FUEL ROD

Fuel Rod Parameters

Fuel material	$(U_{0.75}, Pu_{0.25})O_2$
Pellet density	10.5 g/cm^3
Pellet diameter	0.538 cm (0.212 in.)
Cladding	
Material	316 Stainless Steel
Thickness	0.038 cm (0.015 in.)
Outside diameter	0.635 cm (0.25 in.)

Irradiation History

Irradiated in EBR-II
Cladding temperature - 510-540°C
Discharge date - October 1975
Declared burnup - 179,100 MWd/tU (19.19 atomic percent)

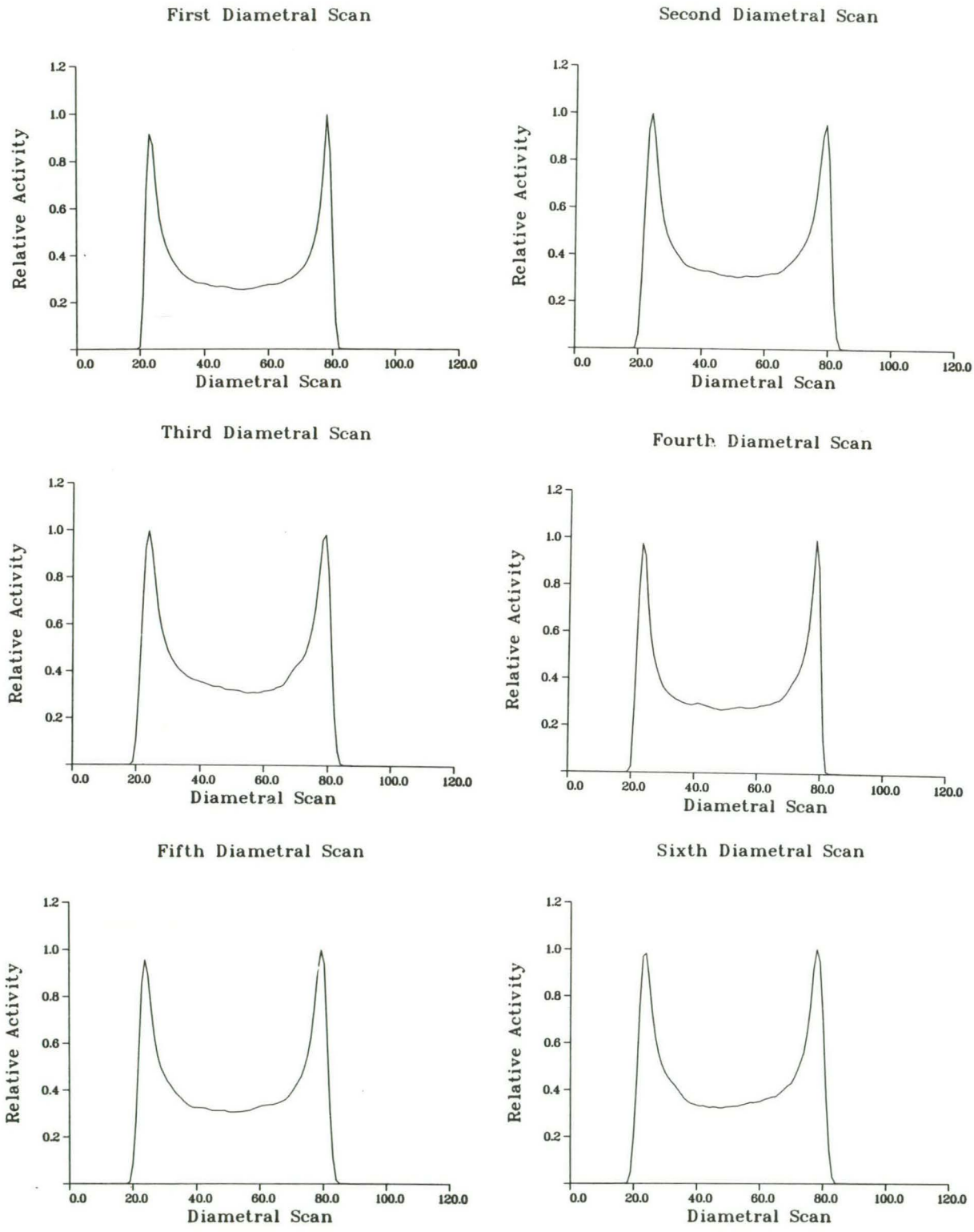

Figure 4-8. Six ^{137}Cs diametral scans (projections) taken at 30° intervals on the FBR fuel rod.

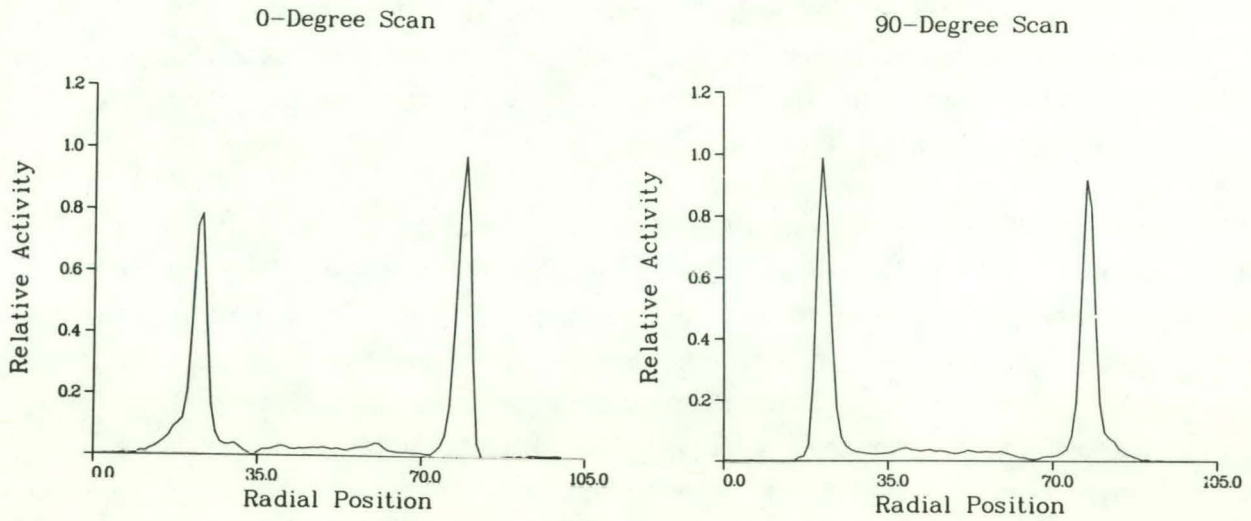

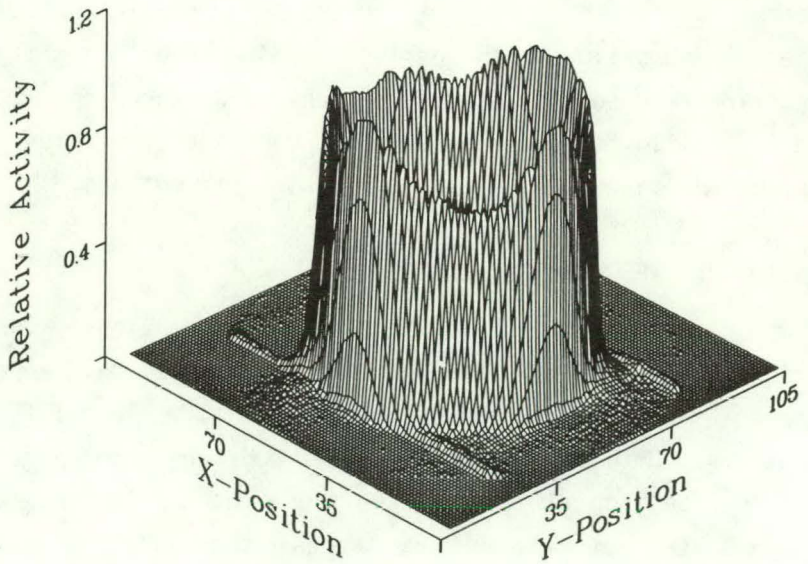

Figure 4-9. The results for ^{137}Cs from the filtered backprojection algorithm including attenuation correction.

order of 0.2 percent. By comparing these radial scan results with the reconstructed results from the fuel cladding activation products shown in Figs. 4-10 and 4-11 for ^{54}Mn and ^{60}Co, respectively, it is clear that the ^{137}Cs is deposited in the pellet clad zone.

The quality of the reconstructions for the ^{54}Mn and ^{60}Co cladding activation products was not as good as the ^{137}Cs reconstruction because of the uncertainty of the input data due to counting statistics. The deviations of the individual data points for the ^{54}Mn data ranged from 5 to 13 percent, with the lower value being on the ring source and the higher value being near the central region of the projection. For the ^{60}Co projection data, the uncertainty in the data ranged from 4 to 9 percent; consequently, the reconstruction of the ^{60}Co is better than the reconstruction of the ^{54}Mn. The problems of the quality of the input projection data are addressed in more detail in Appendix B.

Figures 4-12 and 4-13 show the input projection data and the results for the ^{134}Cs fission product. These results are very similar to the ^{137}Cs results, which is not always the case (26). Counting statistics for these projections ranged from 0.2 to 1.5 percent.

The reconstruction of the ^{125}Sb distribution (Fig. 4-14) shows that it also has moved radially, depositing in the pellet cladding zone. Counting statistics for these projections ranged from 5 to 11 percent. The three results for ^{137}Cs, ^{134}Cs, and ^{125}Sb illustrate the affect that counting statistics can have on the reconstructed images for nearly identical distributions.

D. DISCUSSION OF EXPERIMENTAL RESULTS

The irradiation conditions of this FBR fuel rod are obviously more extreme than the conditions that LWR fuel rods are routinely exposed to. However, it does demonstrate how the technique can be used to identify the relative location of fission products. Both the LWR and FBR fuel rods were cooled for nearly five years; this long cooling time restricted the number of isotopes that could be measured. On other fuel rods we have measured the radial isotopic distribution of fission products with shorter half-lives. A listing of isotopes whose projections have been used to reconstruct the two-dimensional radial distributions is shown in Table III.

We have discussed the importance of counting statistics and their affect on actual and simulated (Appendix B) distributions of gamma-emitting isotopes.

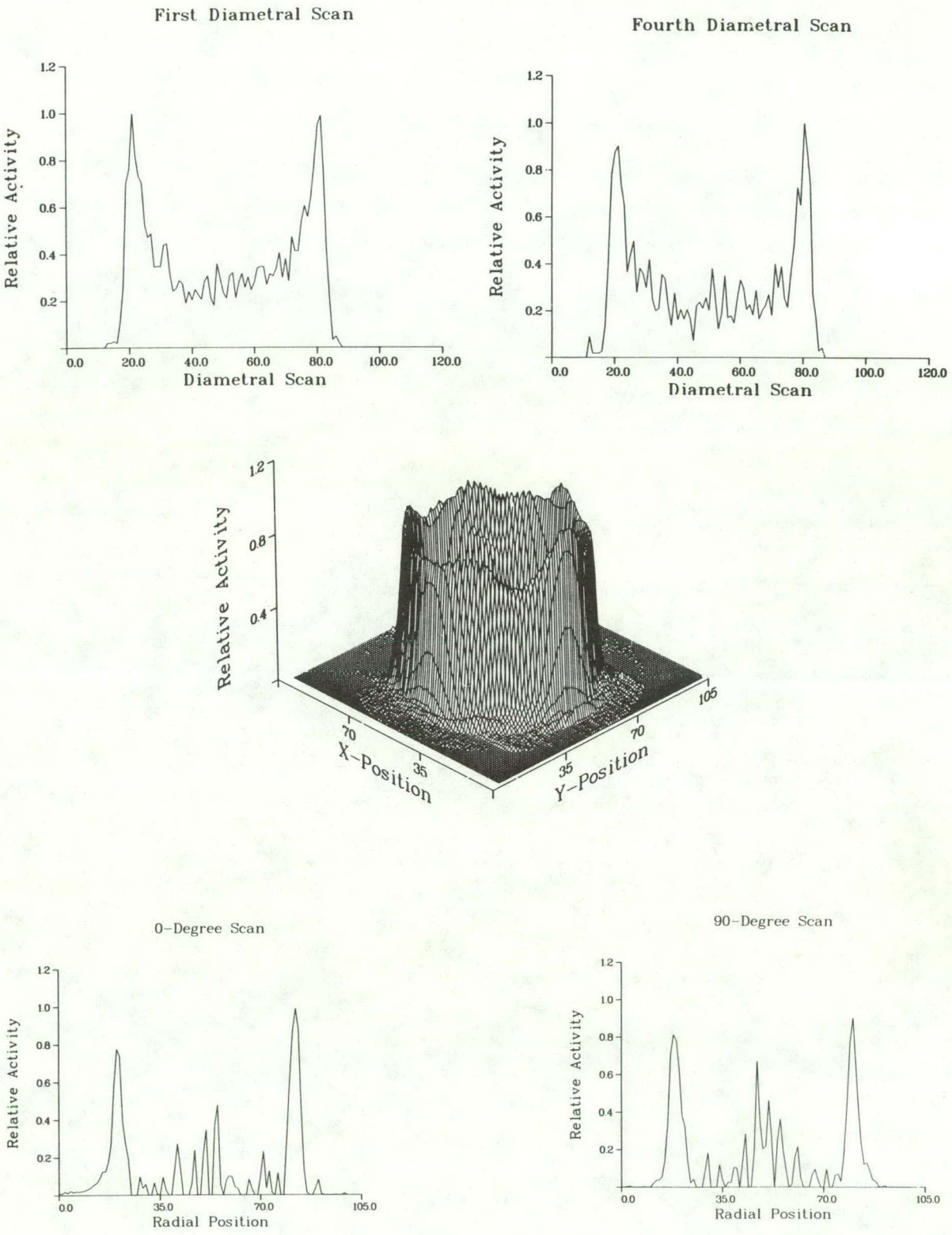

Figure 4-10. Input data and results for ^{54}Mn from the filtered backprojection algorithm including attenuation correction.

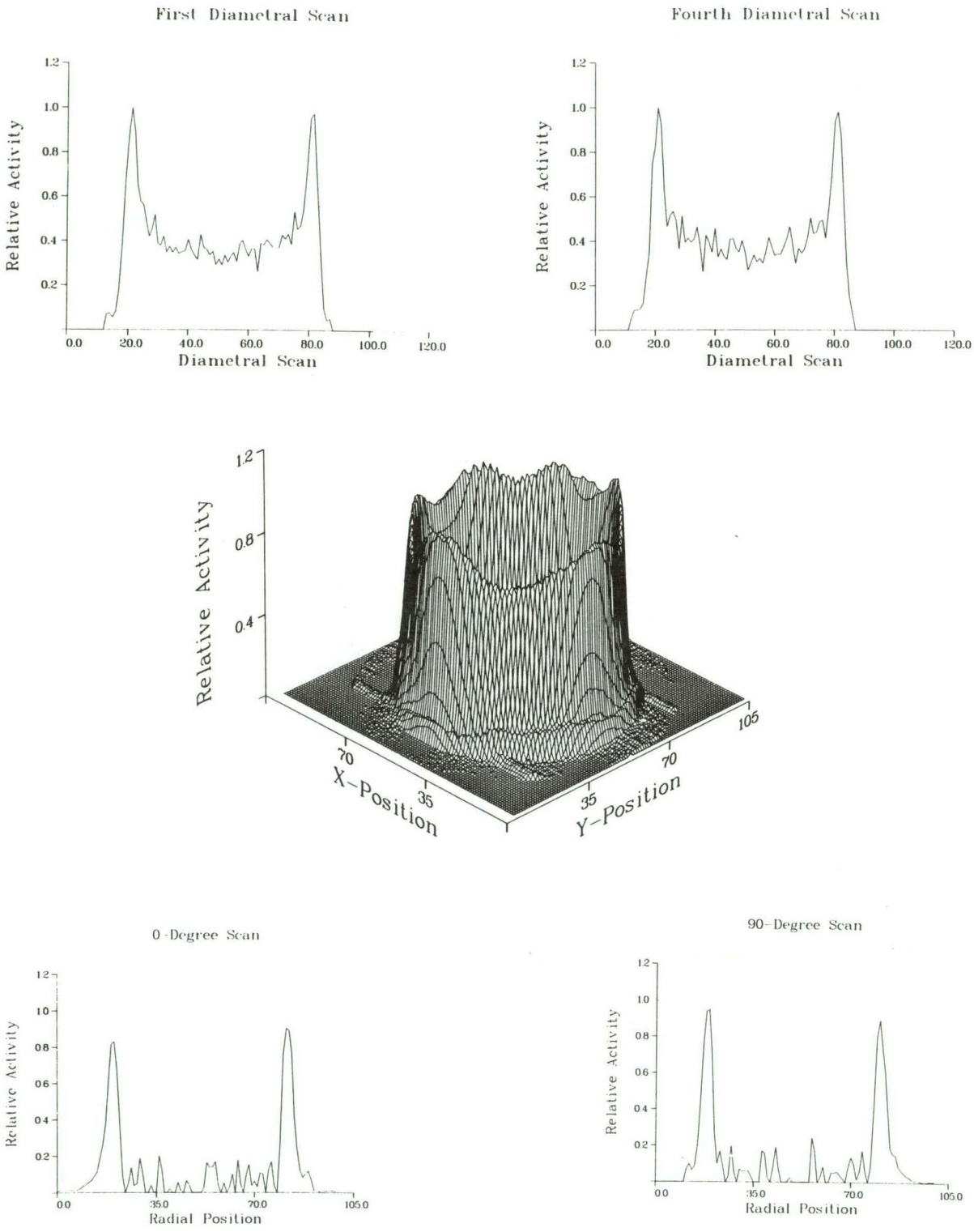

Figure 4-11. Input data and results for ^{60}Co from the filtered backprojection algorithm including attenuation correction.

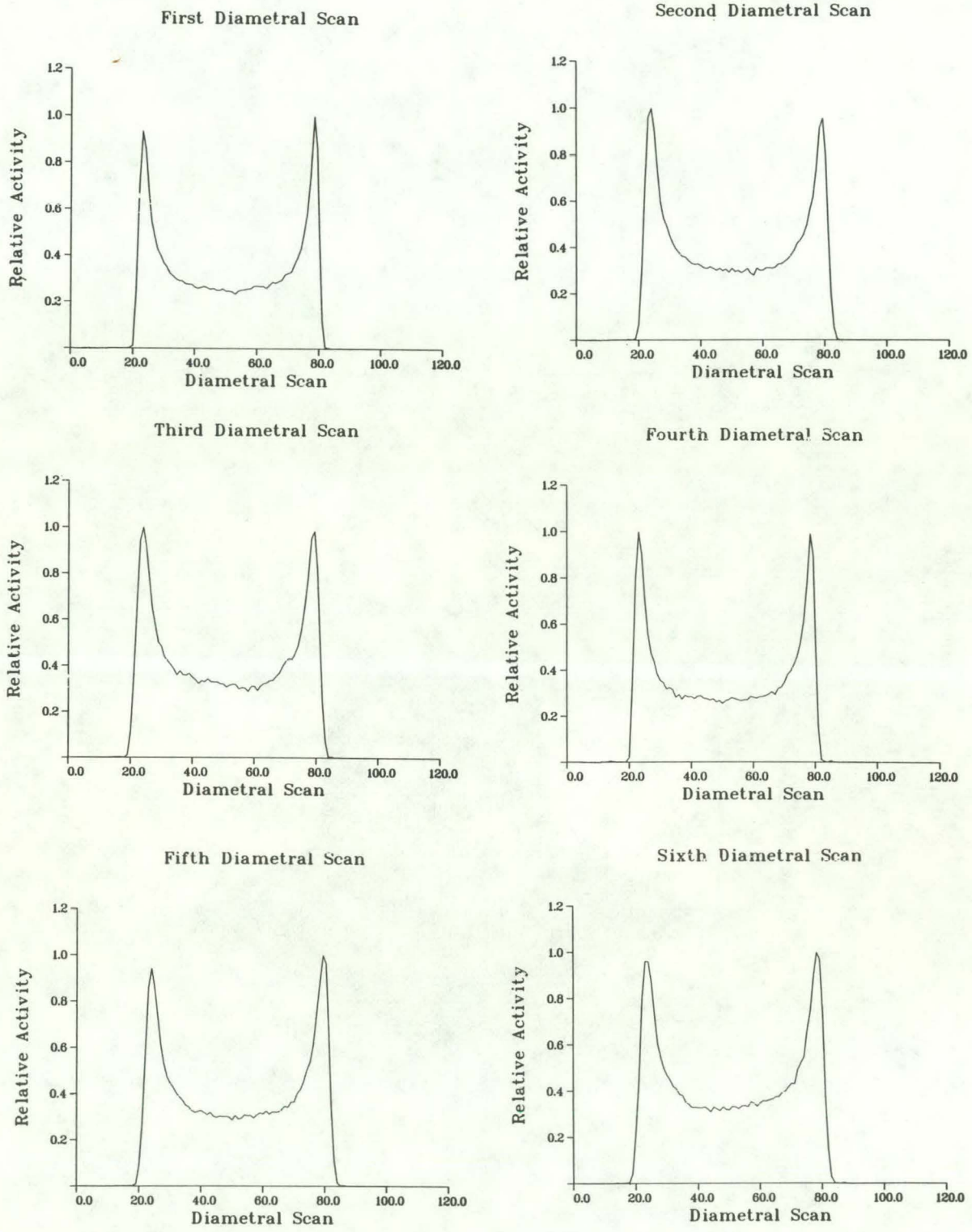

Figure 4-12. Six ^{134}Cs diametral scans (projections) taken at 30° intervals on the FBR fuel rod.

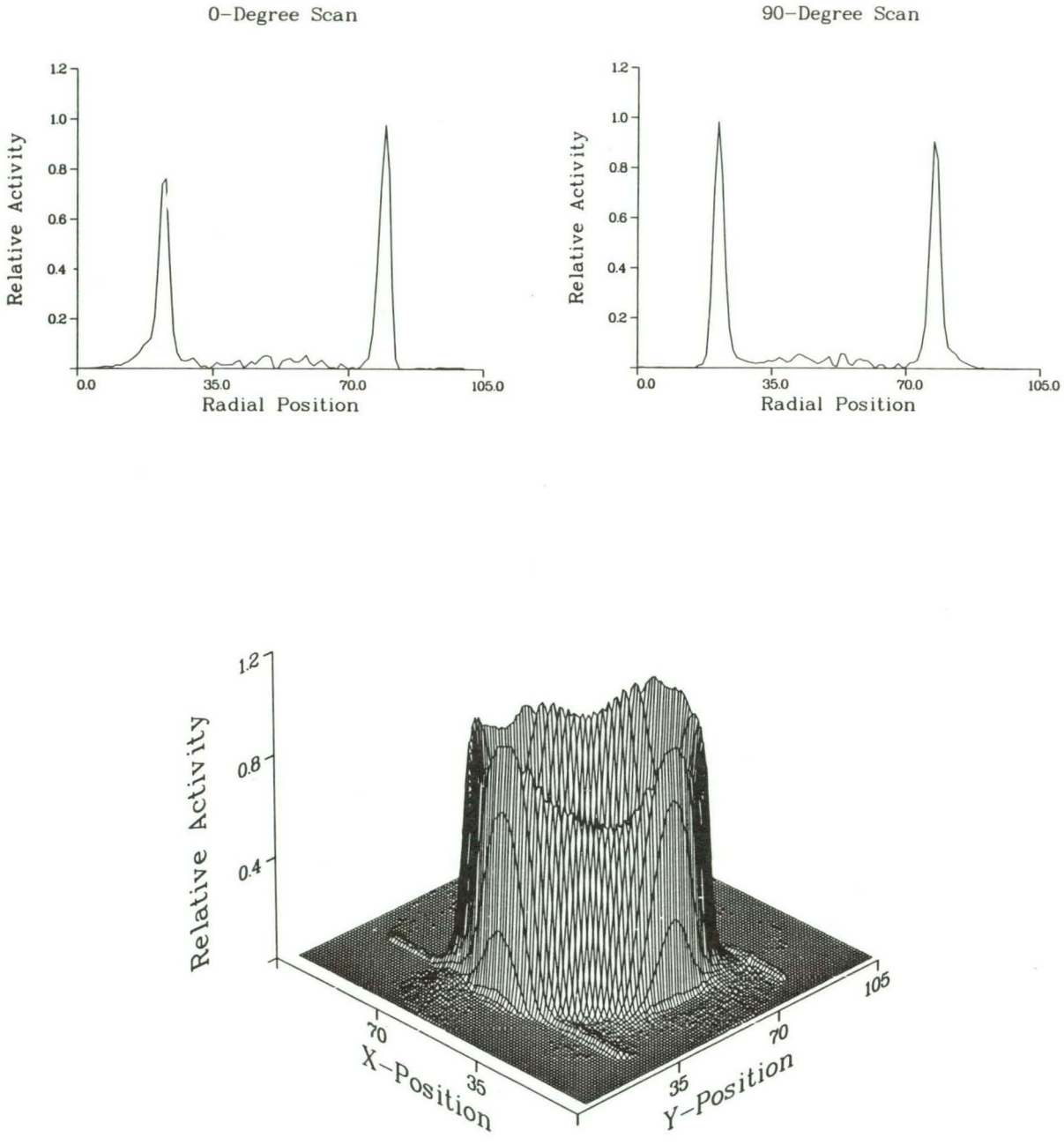

Figure 4-13. The results for ^{134}Cs from the filtered backprojection algorithm including attenuation correction.

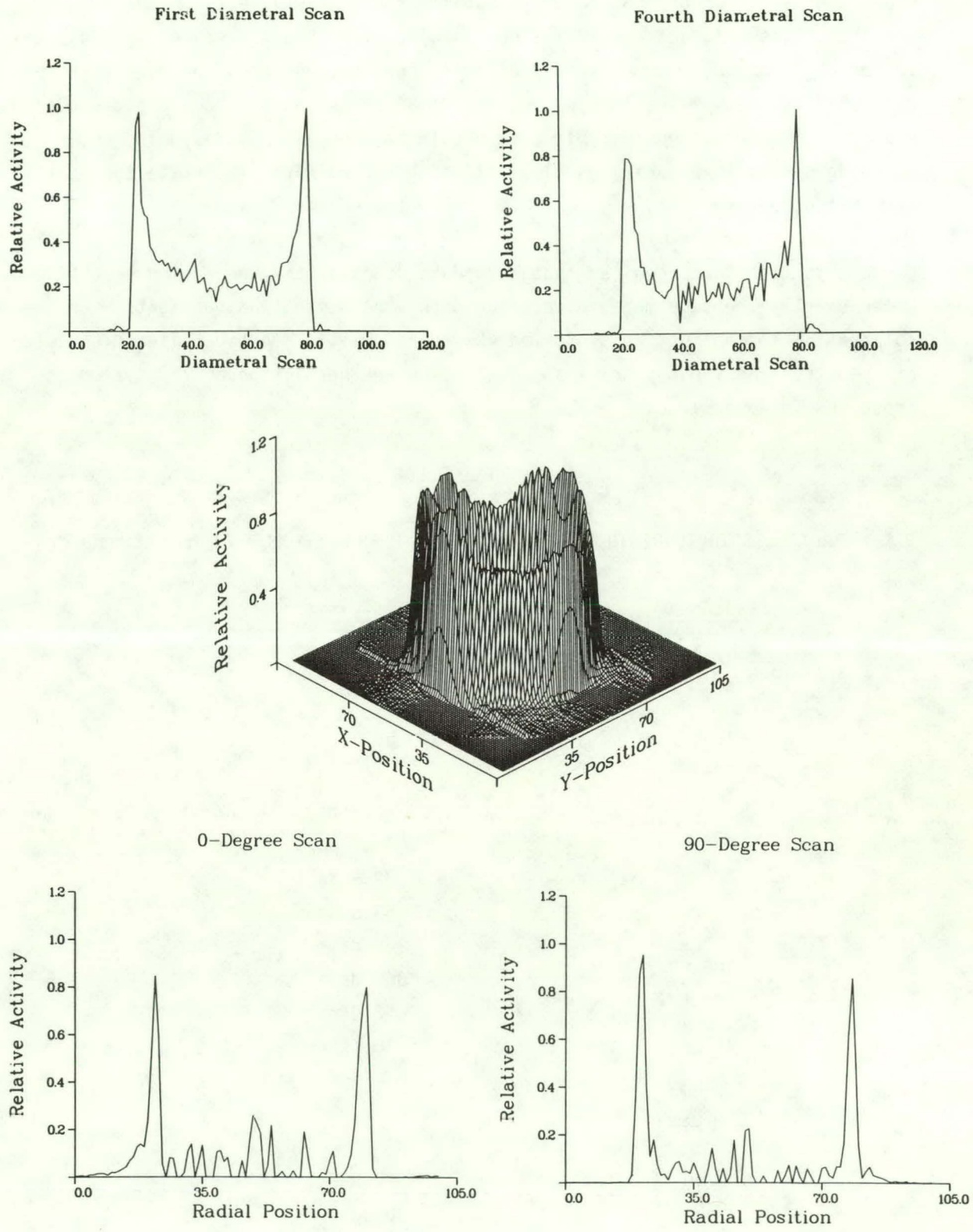

Figure 4-14. Input data and results for ^{125}Sb from the filtered backprojection algorithm including attenuation correction.

Other sources of error that can have equally comparable affects on the results are the errors associated with the positioning of the fuel specimens and changes in the collimation system. The specific reconstruction technique used in these examinations assumes that the projection data (scans) do not have any associated errors. Therefore, considerable care should be exercised in designing the scanning system to ensure minimal positioning errors with respect to the spatial resolution requirements.

Since this technique requires that each data point of the projection be obtained under exactly the same measurement condition, the design and fabrication of the collimation system must be performed very carefully. A more detailed discussion of the effect of various collimating slits on the resolution of the system is presented in Appendix C.

TABLE III

RADIAL ISOTOPIC DISTRIBUTIONS MEASURED USING RECONSTRUCTION TECHNIQUES

Isotopes	Half-Life
Fission Products	
^{132}Te	77.7 h
^{131}I	8.05 days
$^{140}Ba-La$	12.8 days (40.22 h)
^{95}Nb	35.0 days
^{103}Ru	39.5 days
^{95}Zr	65.5 days
$^{144}Ce-Pr$	285 days
$^{106}Ru-Rh$	369 days
^{134}Cs	2.05 yr
^{137}Cs	30.17 yr
Activation Products	
^{51}Cr	27.8 day
^{54}Mn	303 day
^{60}Co	5.26 yr

Section 5

CONCLUSIONS AND RECOMMENDATIONS

Projection data (diametral) of irradiated fuel rods can be used to estimate the actual two-dimensional distribution of fission and activation products. The filtered backprojection reconstruction technique was applied to various test cases, as well as to both LWR and FBR fuel rods. The results demonstrated the type of data that can be obtained using this technique.

The correct design and fabrication of a measurement system, including (1) the scanning mechanism, (2) the collimation assembly, (3) the detector assembly, and (4) the data acquisition and analysis system, are essential to obtain precise projection data. If these components are not correctly integrated into the entire scanning system, the reconstruction algorithm is useless. Therefore, in any implementation program, equal attention should be given to the hardware and software components.

The total cost of a scanning system similar to that described in this paper can range from several hundred thousand dollars to over a million dollars. Prior to the construction of such a system, the investigator must identify the information he expects to obtain so that the design of the system can be optimized. For example, if the deposition of fission products in the pellet-cladding interface zone are of primary interest, then narrow collimating slits and very precise diametral positions are required. On the other hand, if the primary interest is in the interior of the fuel rod, then larger collimating slits can be used (which smear the results more). Once a decision is made about the objectives of a specific system, the design should be simulated to determine if it will provide the desired information. The time permitted for data collection may be the most limiting factor; typically it can take 2-10 hours for each projection depending upon the activity of the fuel specimen and the design of the integrated system. We have simulated our specific scanning geometry at Los Alamos using Monte Carlo simulation techniques (27) to the total response of the gamma scanning system. Similar calculational techniques can be applied to any conceptual design to assess its advantages and limitations.

This system could be applied to a variety of fuel characterization problems: investigation of fission products in the pellet-cladding interaction zone, measurement of radial power levels in fuel rods, and measurement of experimental or standard fuel irradiated under nonroutine conditions. This technique is the only one available for measuring nondestructively the distribution of fission and activation products within irradiated fuel materials.

APPENDIX A

SIMULATED GAMMA-RAY EMISSION SOURCES

A computer code was written to simulate the projections of emission sources for testing the various unfolding and reconstruction techniques. This code has the capability of generating ring, solid, or combination sources that can be skewed across the diameter at any angle. Another option permits the transformation of perfect data to data having a normal distribution with a specified standard deviation; this option was used in Appendix B to demonstrate the affect of changes in counting statistics on the reconstructed data.

Basically, seven test cases were used to evaluate the applicability of the specific reconstruction techniques. The individual test cases are listed in Table A-1. Six projections separated by 30° were generated for each of the seven test cases.

Figures A-2, -4, -6, -8, -10 and -12 show the reconstructed images resulting from use of the filtered backprojection technique on the data given in Figs. A-1, -3, -5, -7, -9, and -11. The backprojection algorithm appears to have done an excellent job on reconstructing the original images in all six test cases, as well as in the simulated cesium example described in the Section 4.

TABLE A-1

SIMULATED GAMMA-RAY SOURCES

Type	Figure Number	Description
Perfect cylinder	A-1	Simulates a uniformly distributed source
Skewed cylinder - 90 percent	A-3	Simulates a source that varies by 90 percent across the diameter of the scan region
Skewed cylinder - 20 percent	A-5	Simulates a source that varies by 20 percent across the diameter of the scan region
Perfect ring	A-7	Simulates a uniformly distributed ring source that has a width of 6 percent of the total radius
Skewed ring - 90 percent	A-9	Simulates a uniformly distributed ring source that has a width of 6 percent of the total radius but is skewed by 90 percent across the diameter of the scan region
Skewed ring - 20 percent	A-11	Simulates a uniformly distributed ring source that has a width of 6 percent of the total radius but is skewed by 20 percent across the diameter of the scan region
Cesium simulation	2	Described in the Results Section

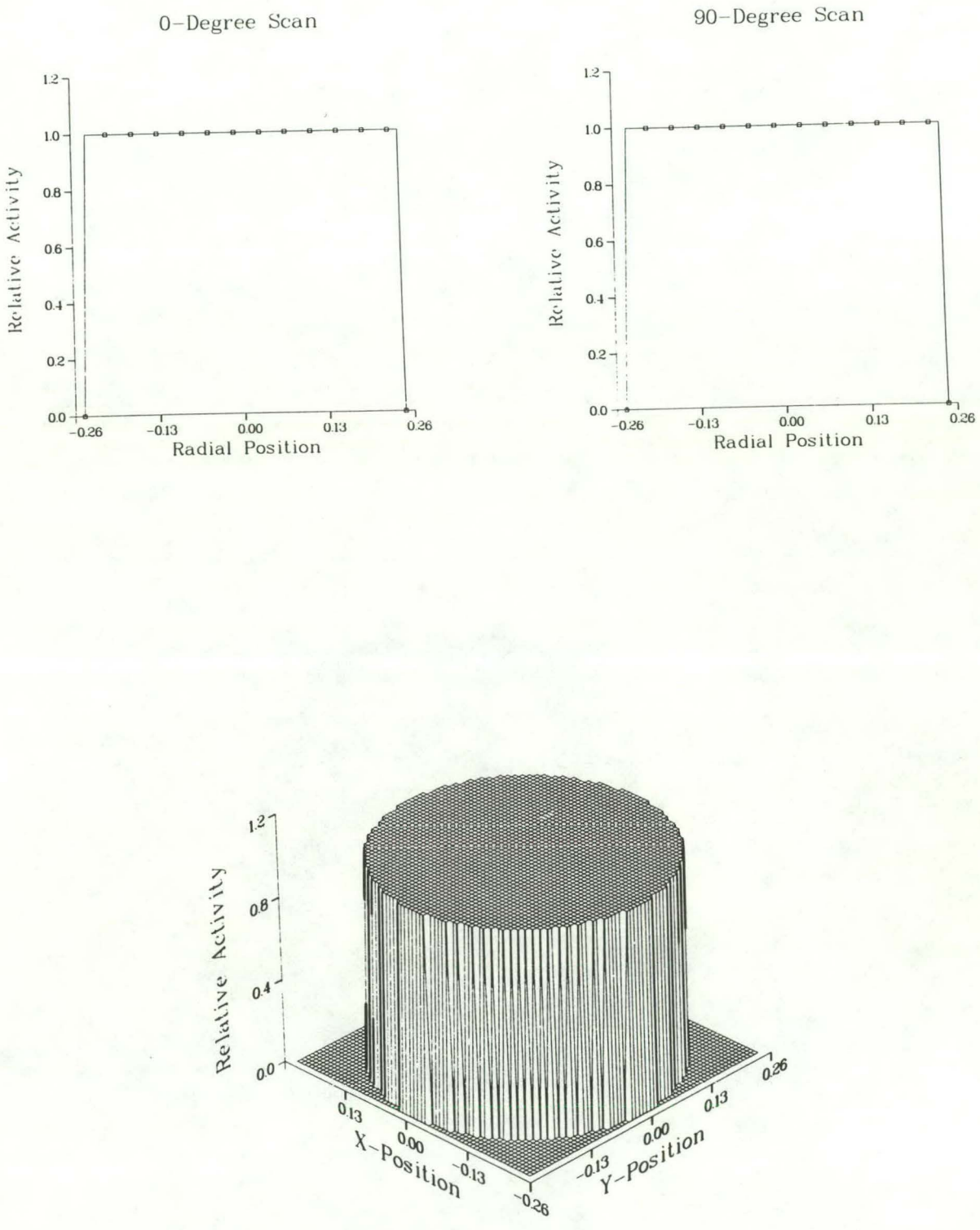

Figure A-1. Perfect uniform source simulating a uniformly distributed source.

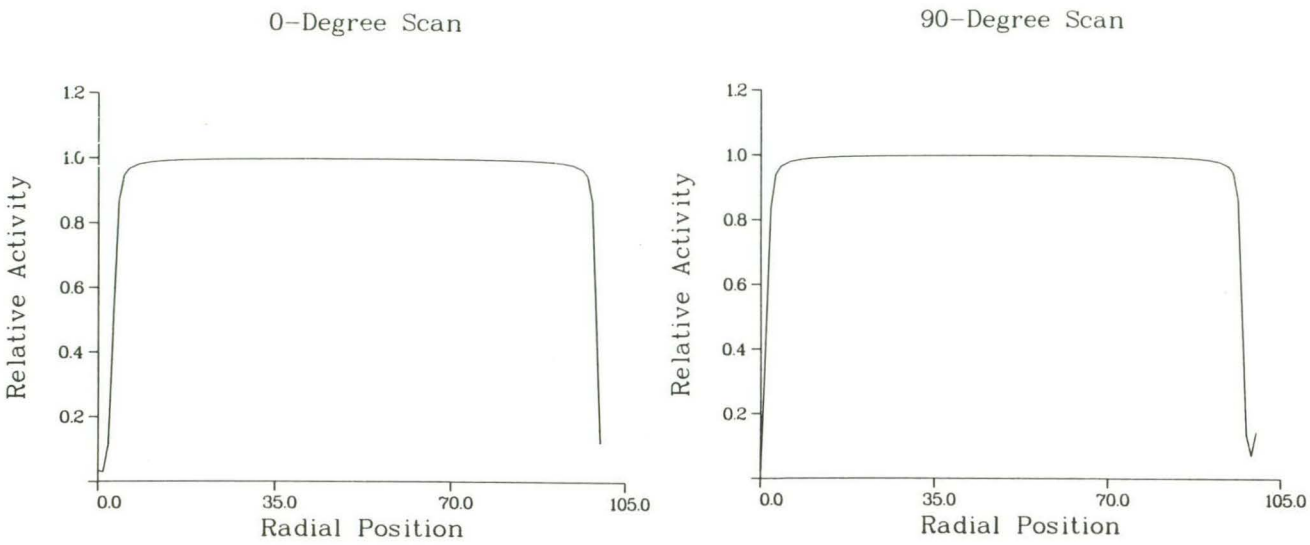

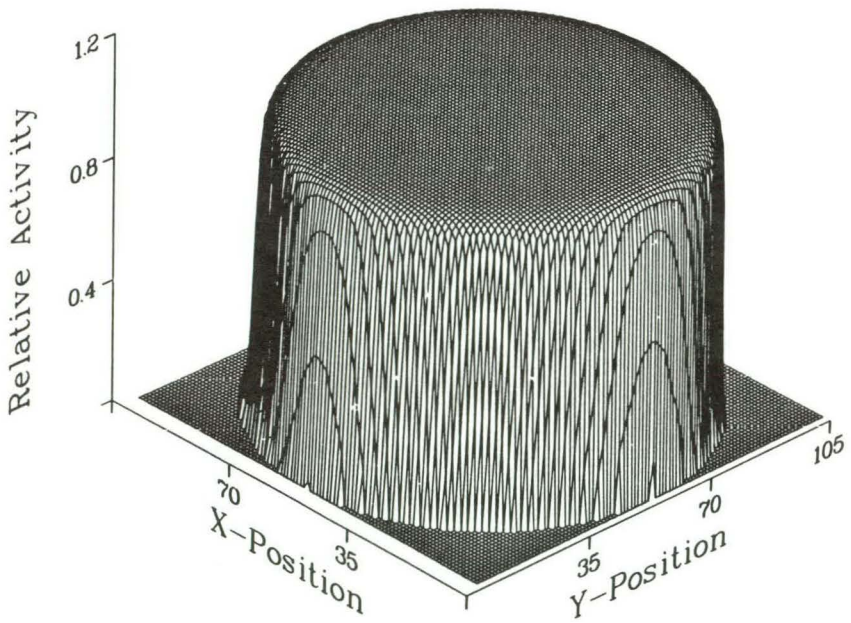

Figure A-2. Filtered backprojection results for the data in Fig. A-1.

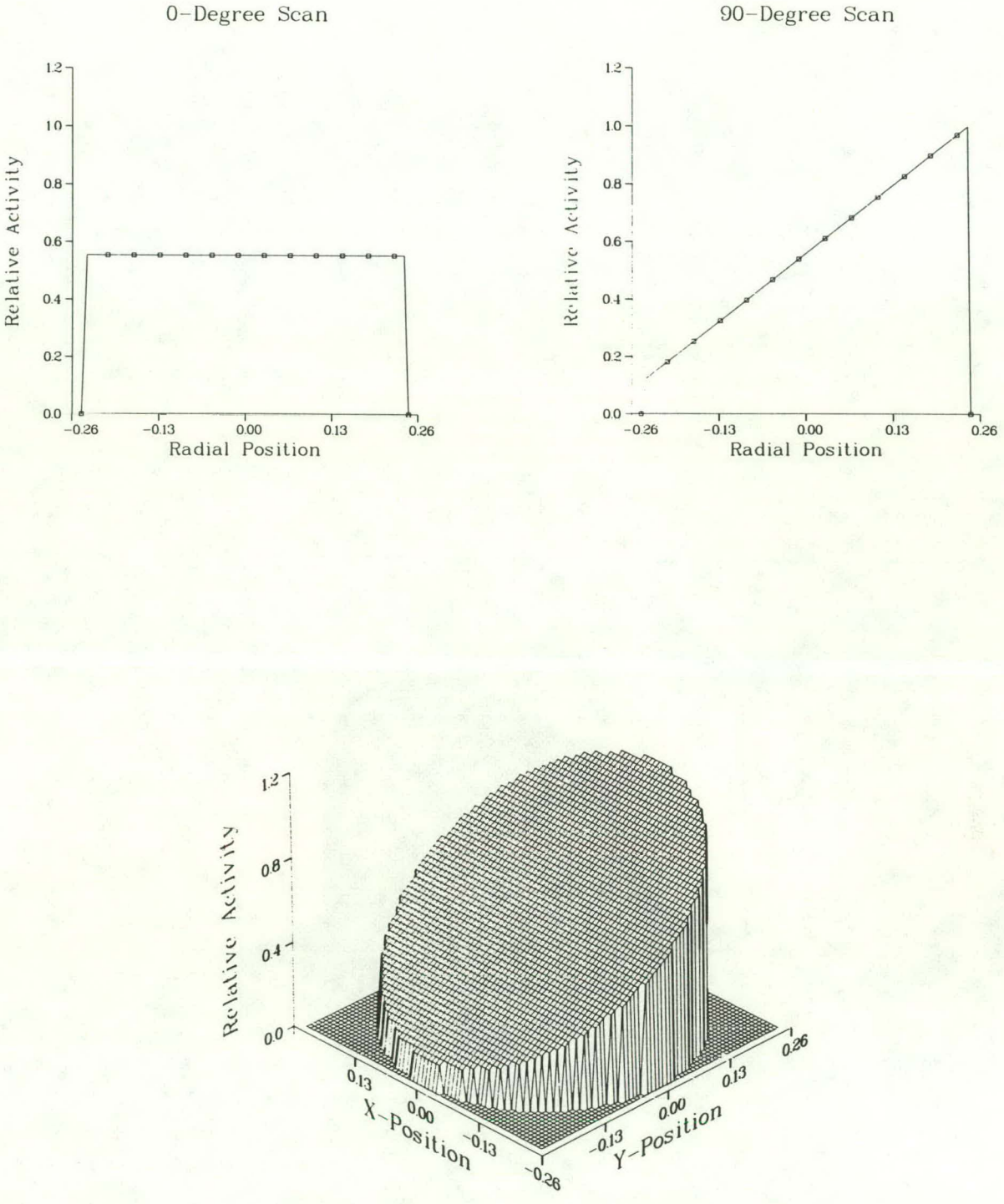

Figure A-3. Skewed uniform source that varies 90 percent across the scan region.

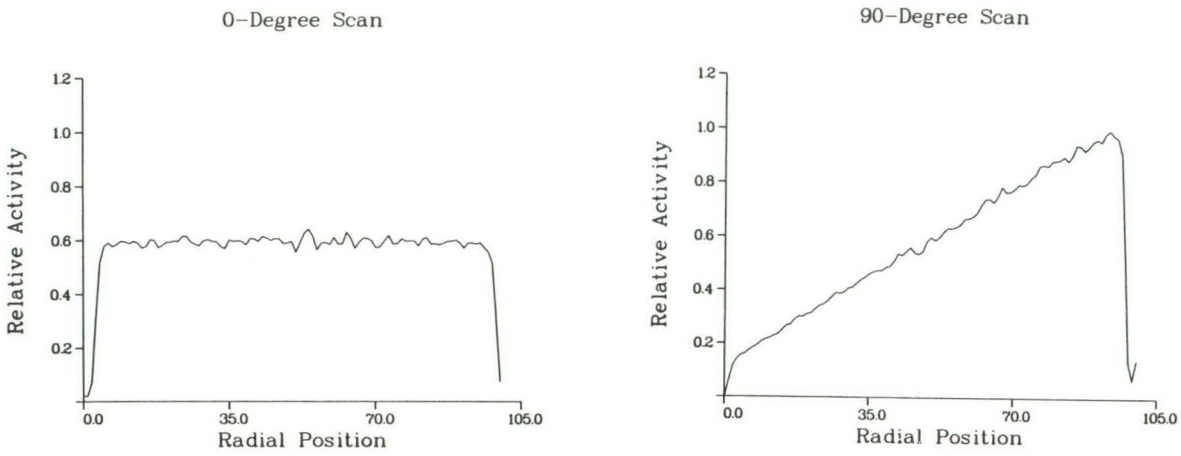

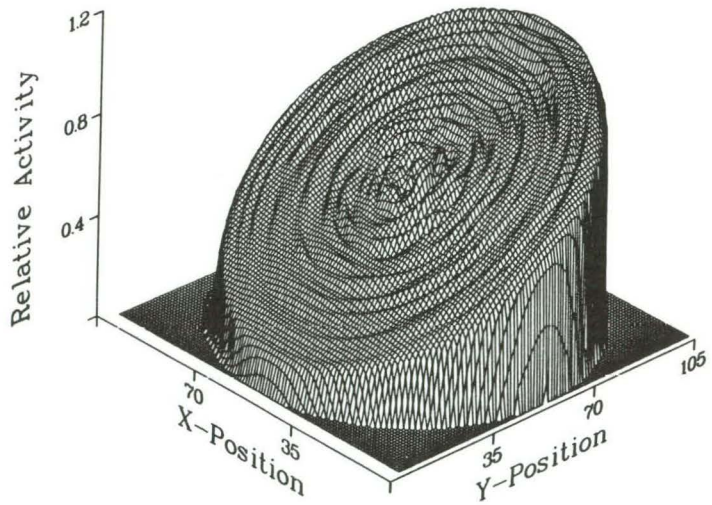

Figure A-4. Filtered backprojection results for the data in Fig. A-3.

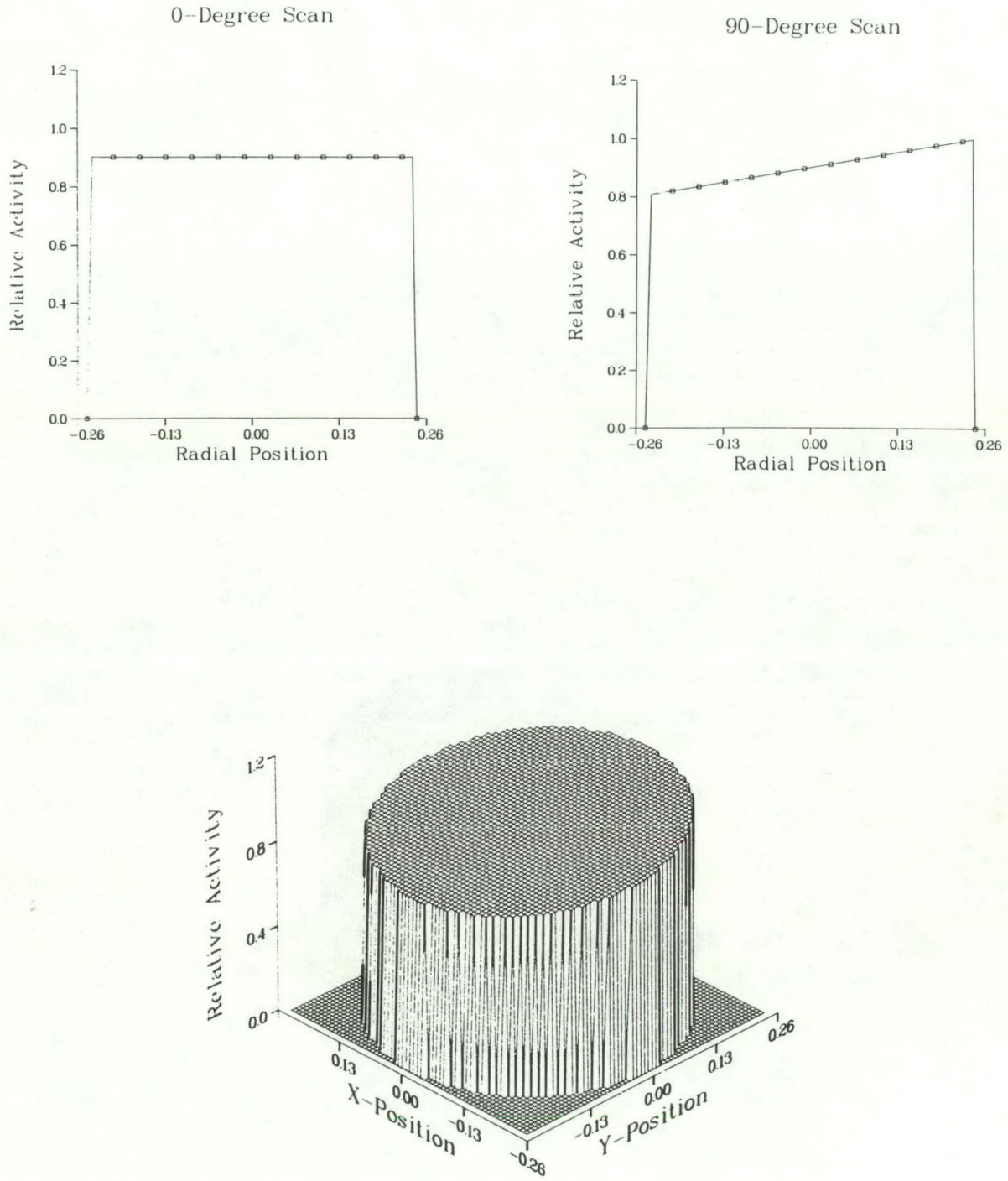

Figure A-5. Skewed uniform source that varies 20 percent across the scan region.

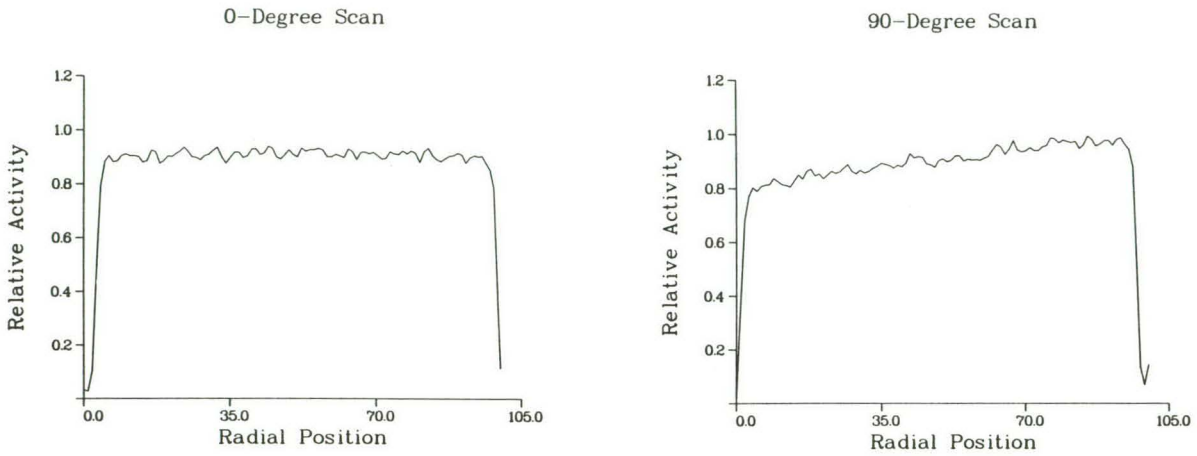

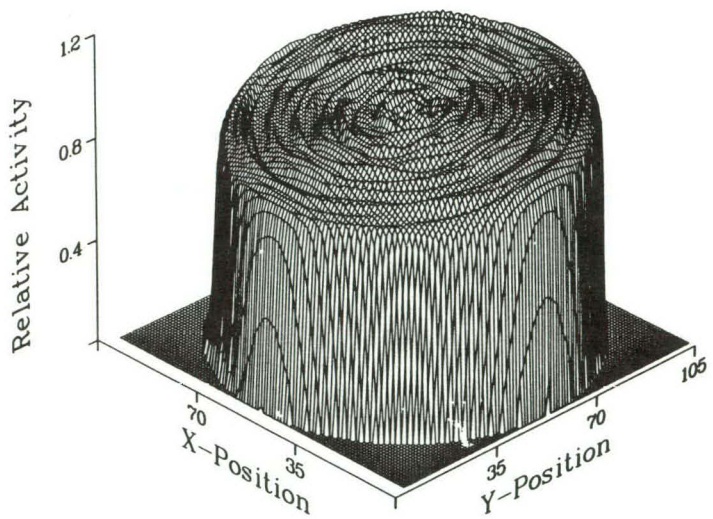

Figure A-6. Filtered backprojection results for the data in Fig. A-5.

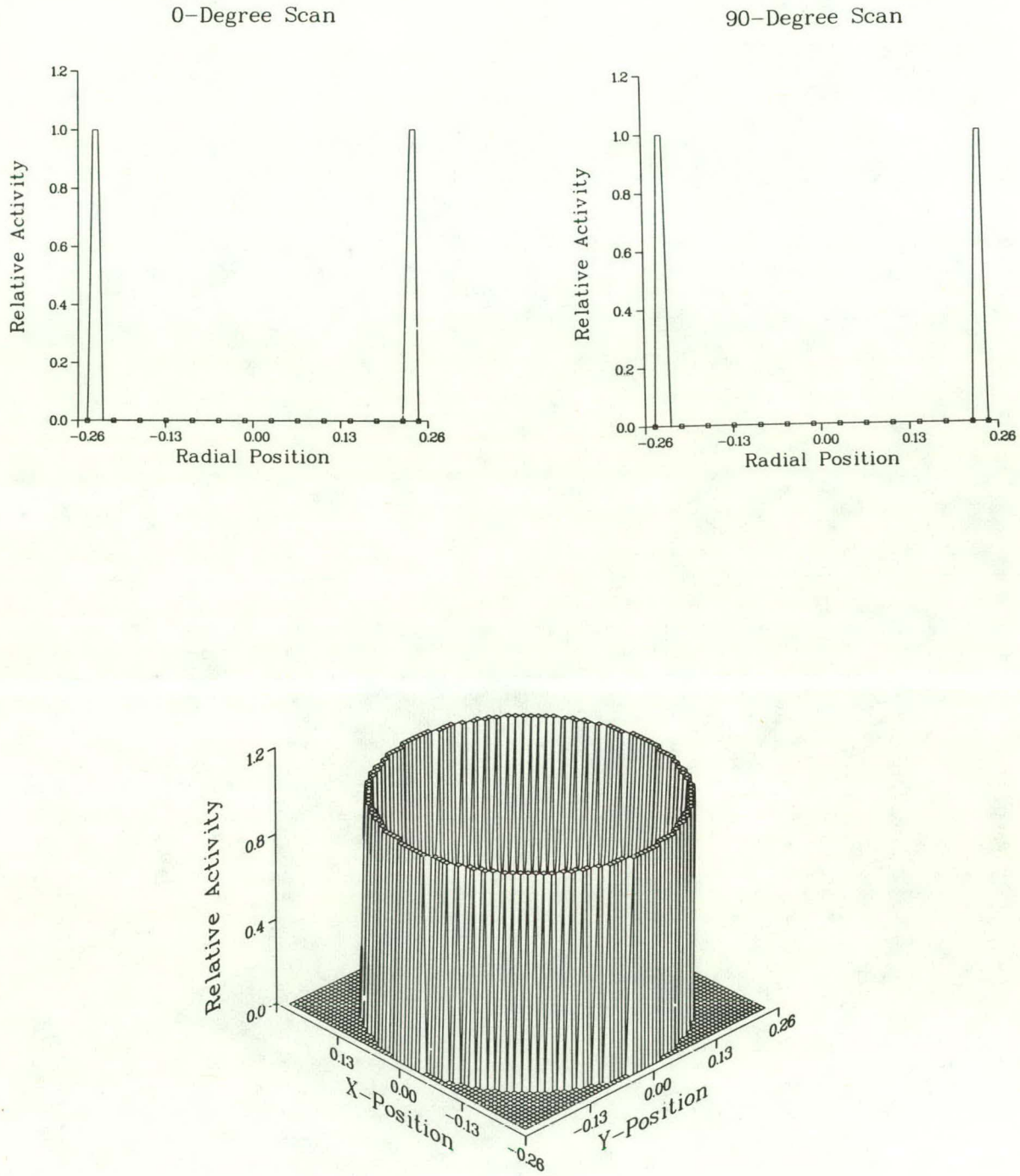

Figure A-7. Perfect ring source with a width 6 percent of total scan region.

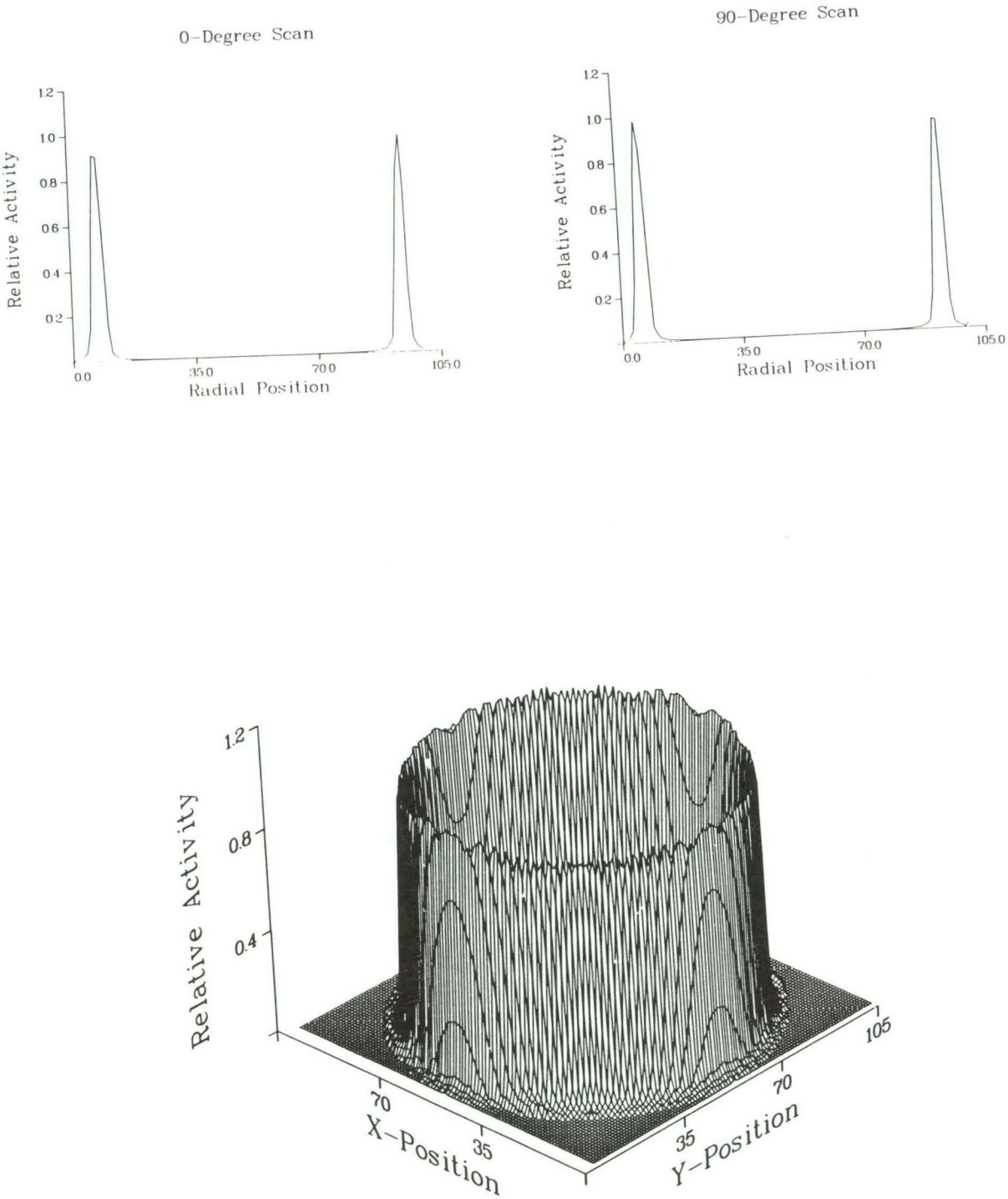

Figure A-8. Filtered backprojection results for the data in Fig. A-7.

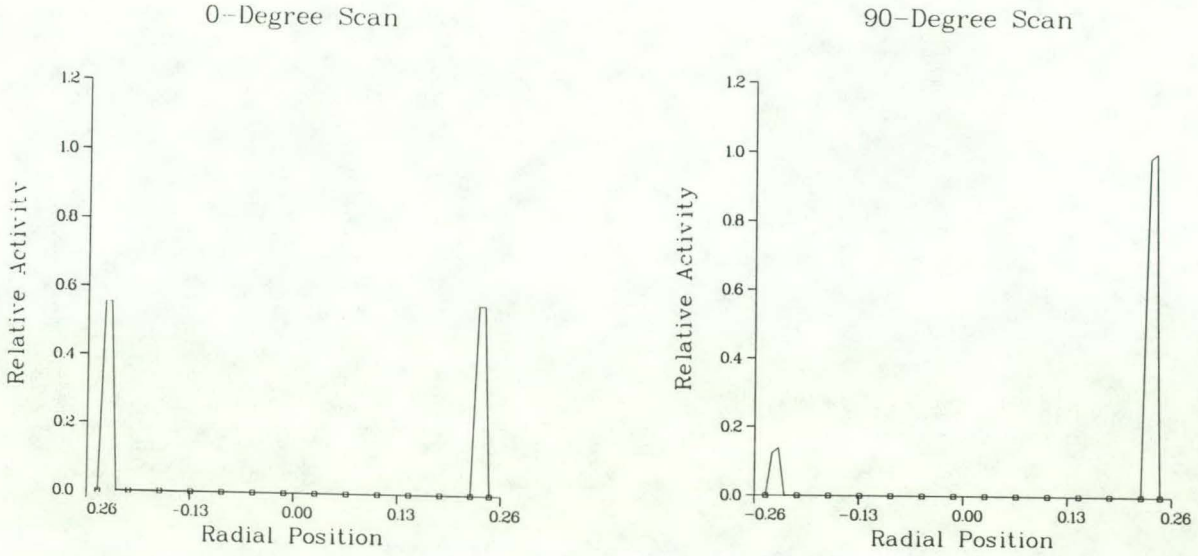

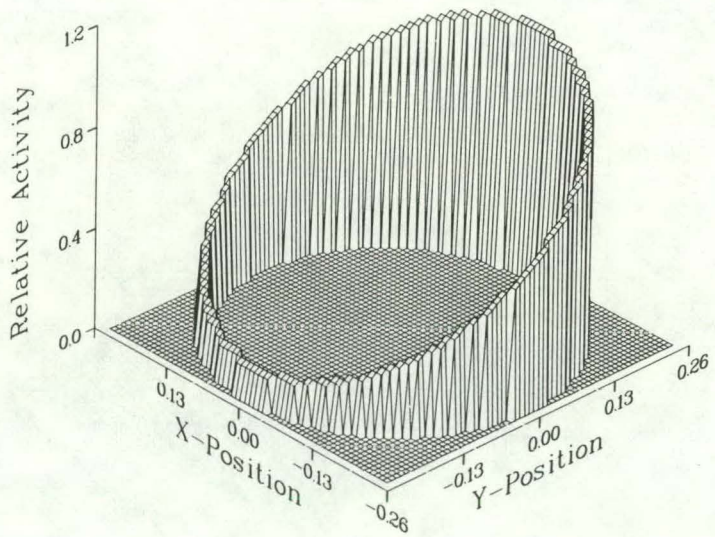

Figure A-9. Skewed ring source that varies 90 percent across the scan region.

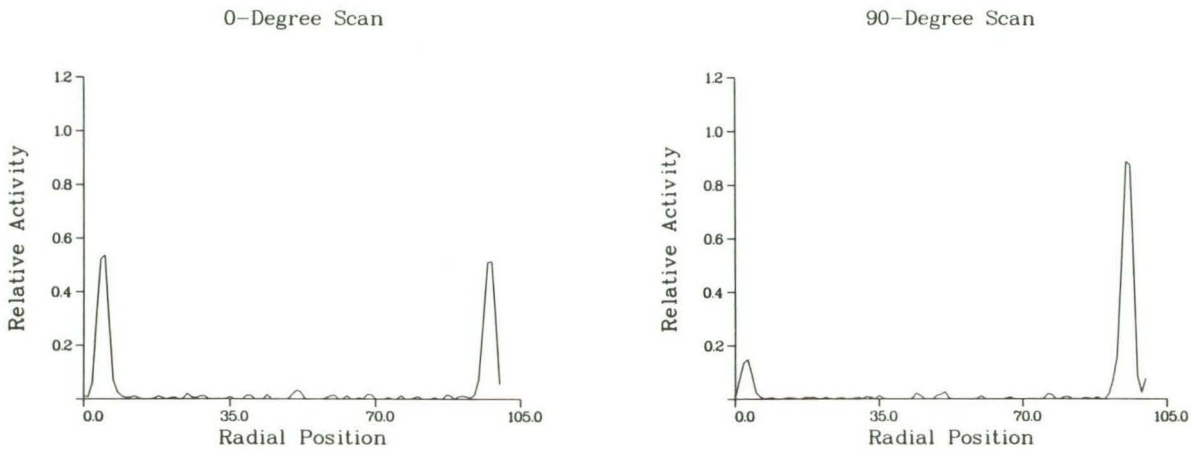

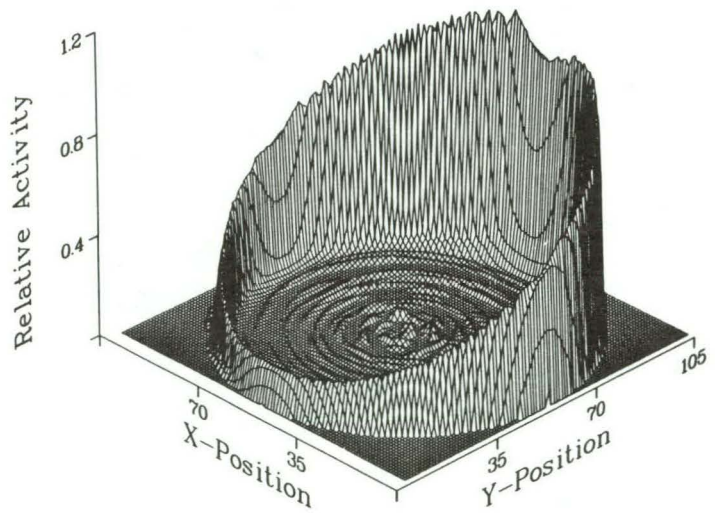

Figure A-10. Filtered backprojection results for the data in Fig. A-9.

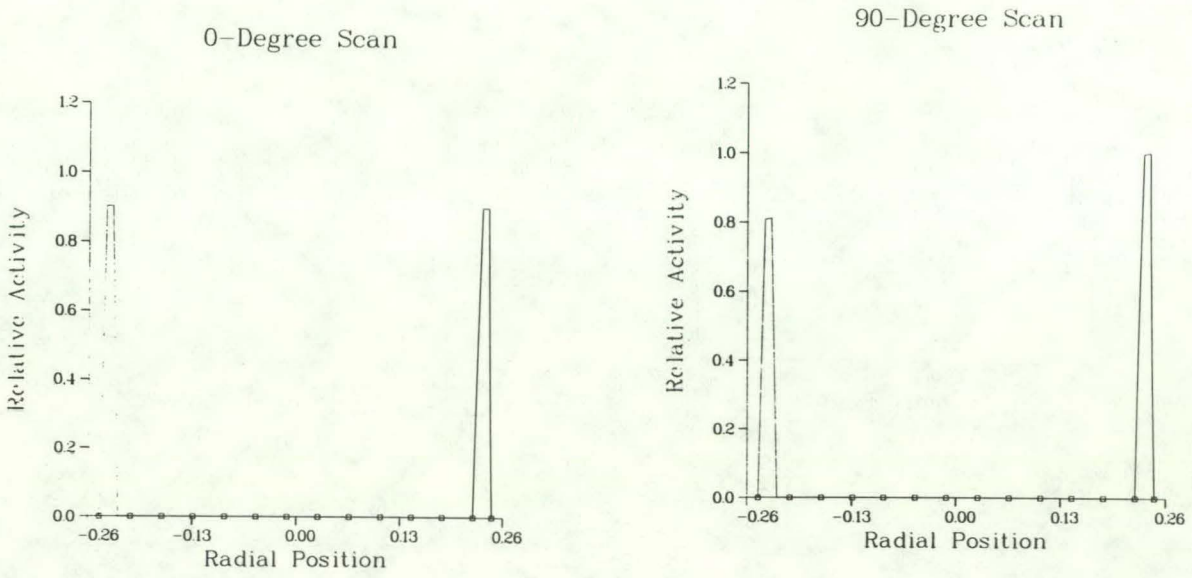

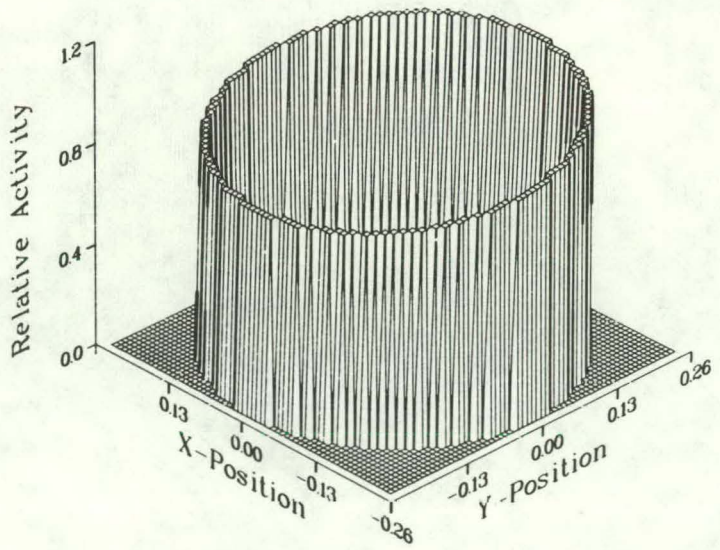

Figure A-11. Skewed ring source that varies 20 percent across the scan region.

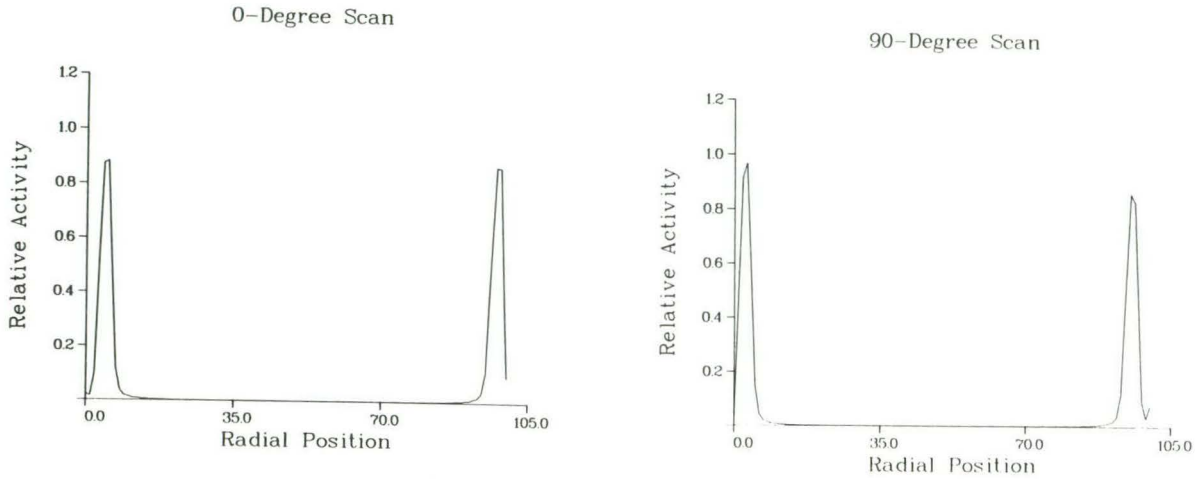

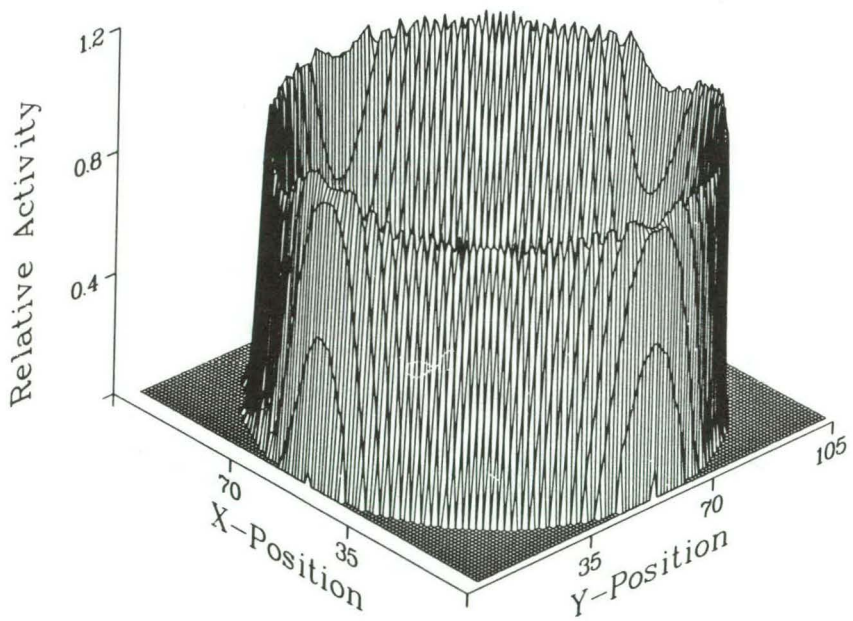

Figure A-12. Filtered backprojection results for the data in Fig. A-11.

APPENDIX B

EFFECT OF COUNTING STATISTICS ON THE FILTERED BACKPROJECTION ALGORITHM

The computer code TWOCHK was used to generate simulated projection data having various levels of counting statistics based upon a normal distribution of errors. Four test cases are presented in Figs. B-1 through B-4 for a uniform source and a ring source, with no errors and 0.2-percent, 1.0-percent, and 2.0-percent errors. The seed of the random numbers generator was identical for each set of the projections; that is, the functional variation for the uniform source test case was identical, except that the magnitude of the deviation changed. In each test case, six projections were used in the reconstruction algorithm with the interpolation described in Section 4, Results.

As is evident from the two test cases, the counting statistics can have a significant influence on the resulting reconstruction. However, it should be stressed that to perform a set of measurements on a fuel section, a finite period of time can be expended. Instead of concentrating on obtaining very good statistics on a few scans, it may be more beneficial to obtain more projections with poorer statistics. Additional calculational and experimental work should be performed to determine the trade-offs between the two data collection approaches.

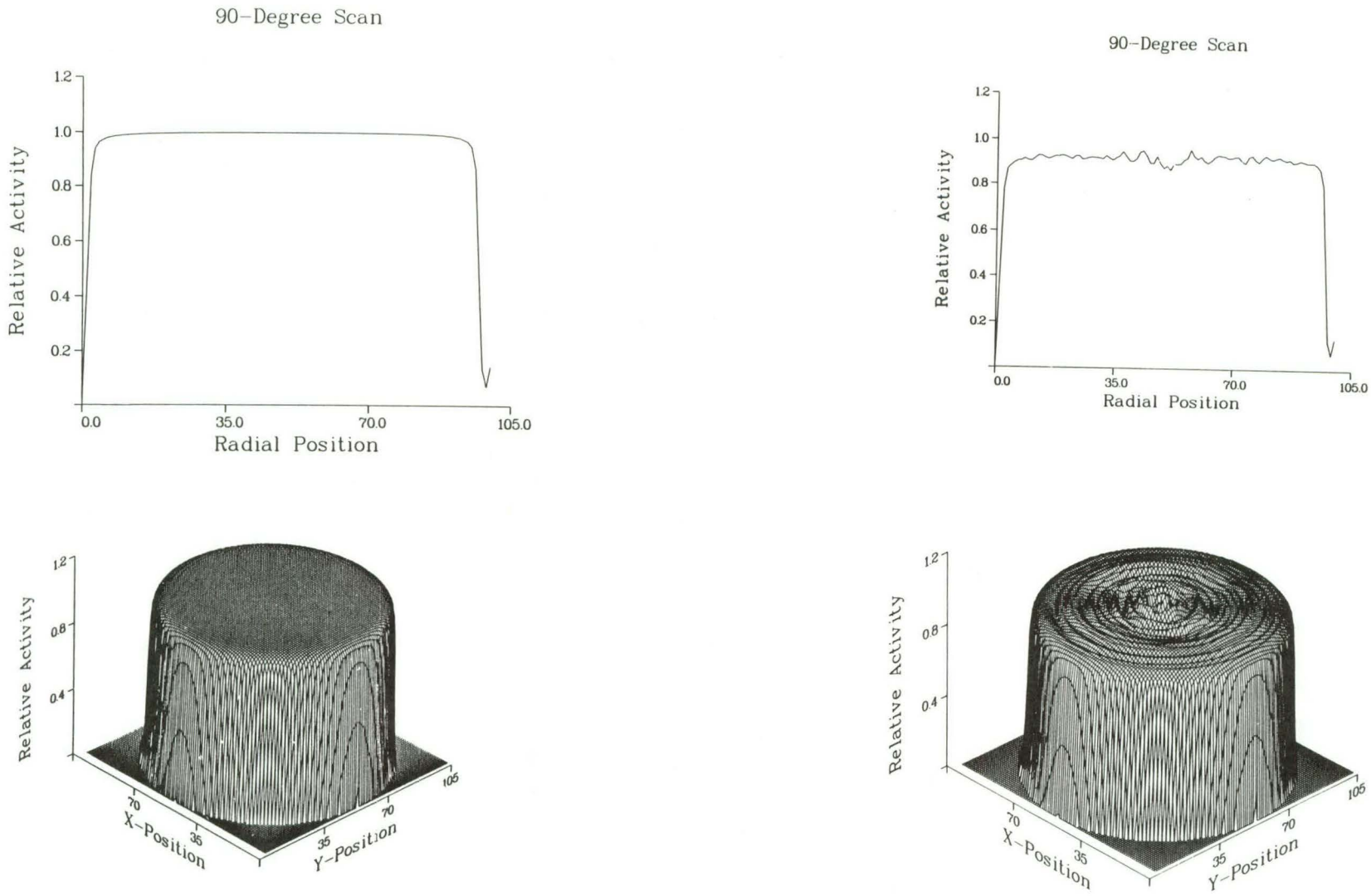

Figure B-1. Results for perfect and 0.2 percent error data using the filtered backprojection algorithm on a uniform source.

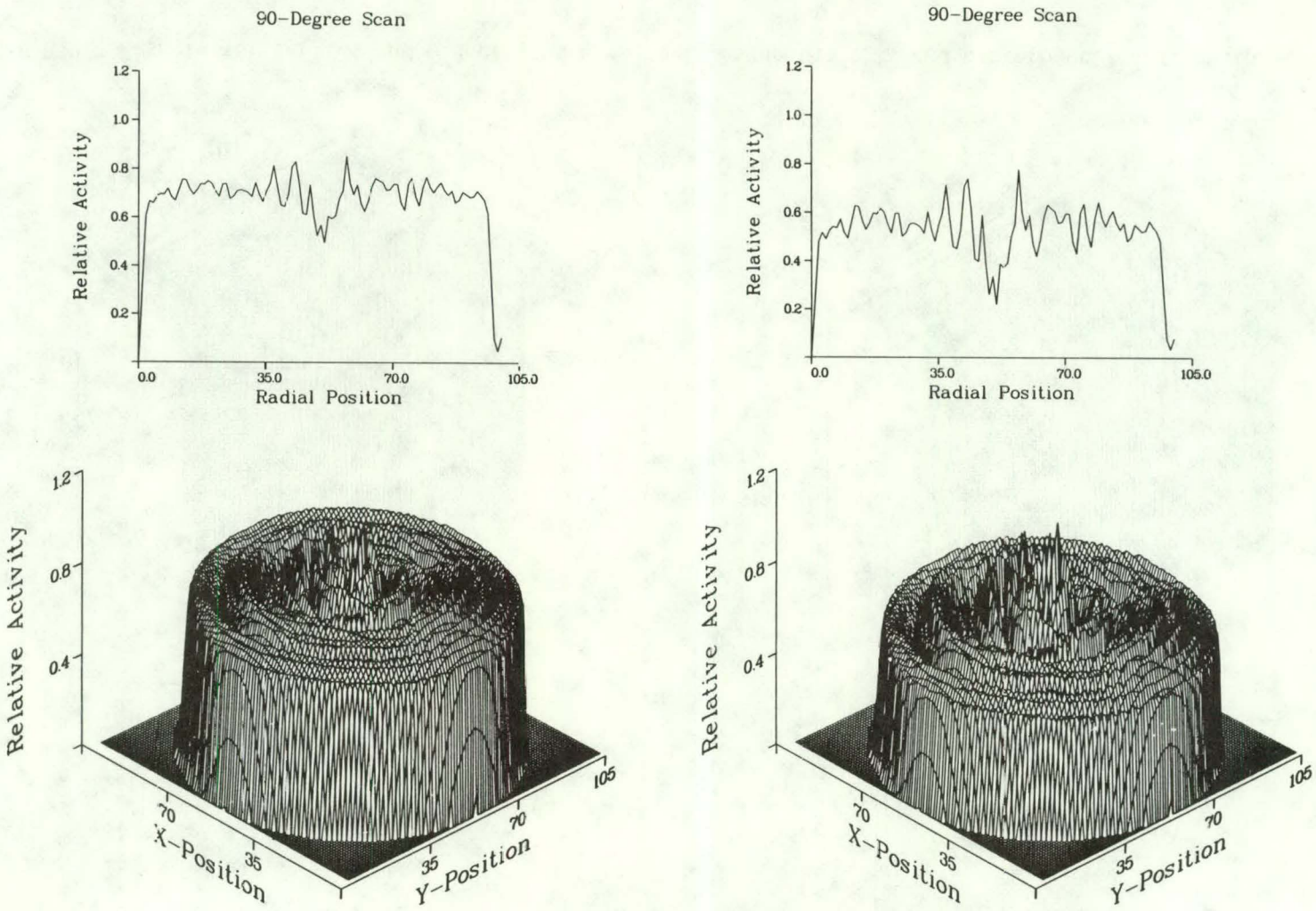

Figure B-2. Results for 1 percent and 2 percent error data using the filtered backprojection algorithm on a uniform source.

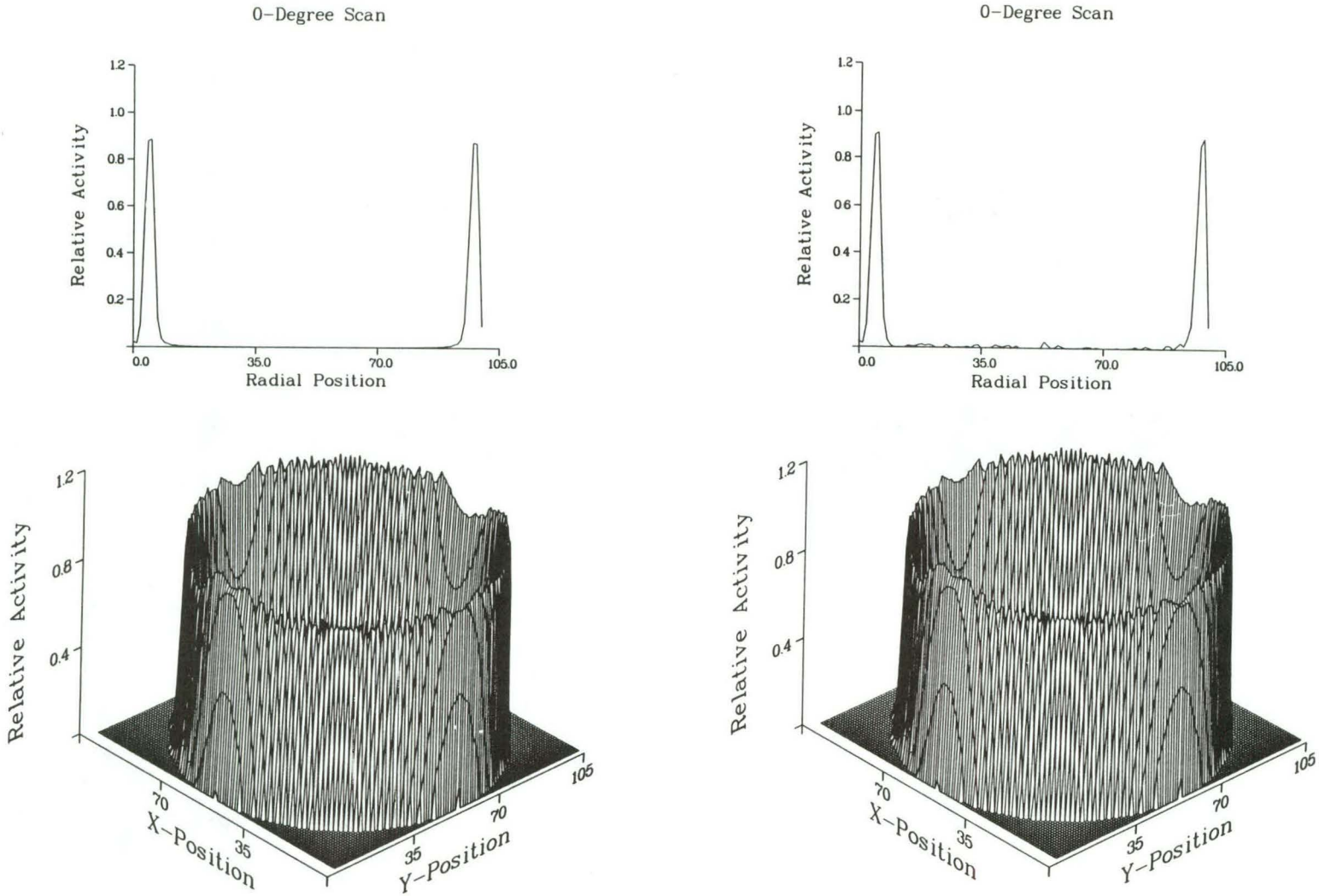

Figure B-3. Results for perfect and 0.2 percent error data using the filtered backprojection algorithm on a ring source.

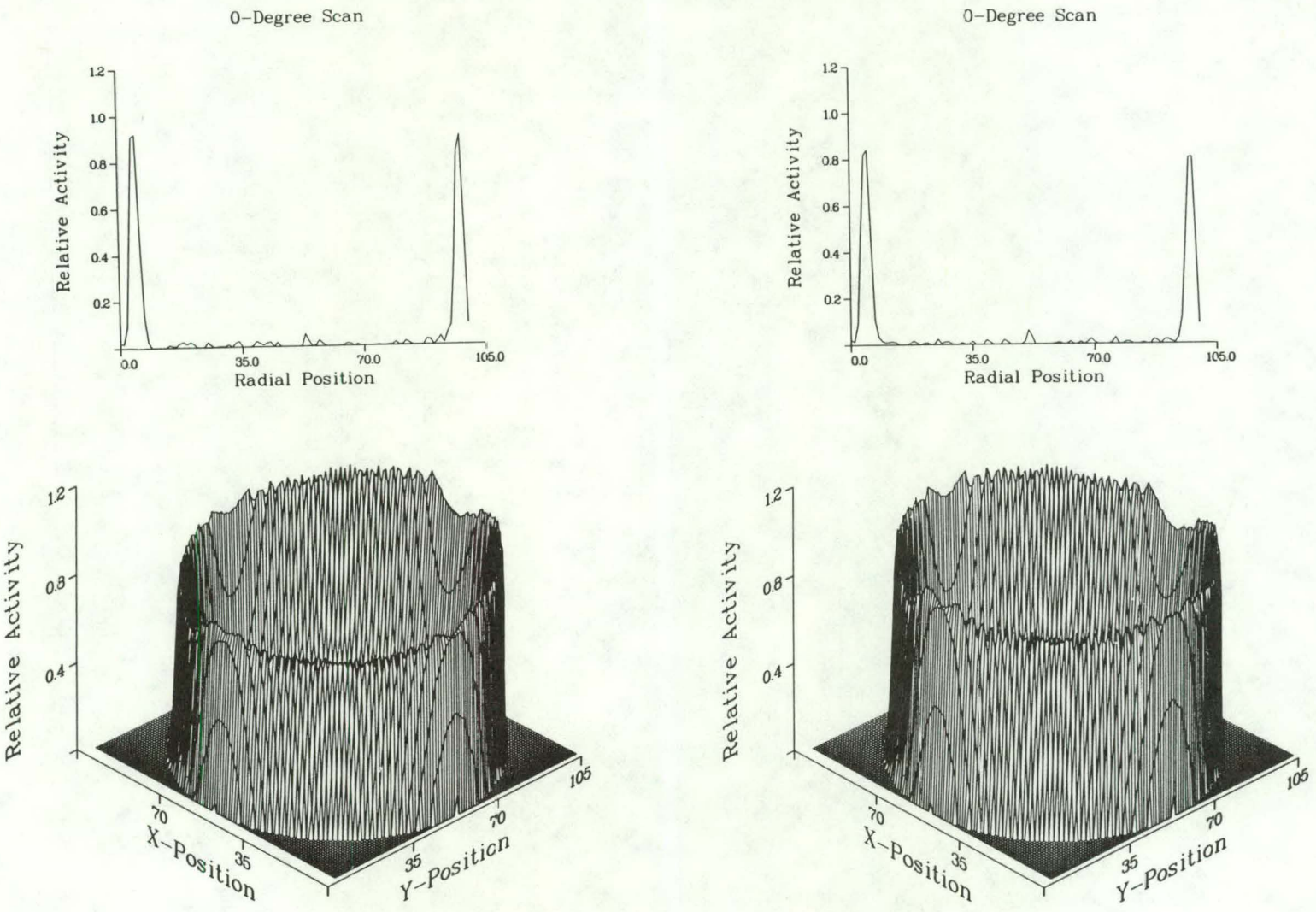

Figure B-4. Results for 1 percent and 2 percent error data using the filtered backprojection algorithm on a ring source.

APPENDIX C

EFFECT OF SLIT SIZE ON SPATIAL RESOLUTION

The TWOCHK computer code was used to generate two idealized source distributions--a uniform source and a ring source--which were scanned calculationally to simulate various slit sizes. Four slit widths were used: 0.0127, 0.0254, 0.0505, and 0.127 cm. Each collimating slit was moved in 0.0127-cm steps across the two idealized source distributions. The results for the various slit sizes on the uniform source and the ring source are shown in Figs. C-1 and C-2. Increasing the collimating slit size does not significantly alter the uniform source distribution; however, changing the slit sizes alters the projections for the ring source.

Similar effects of varying the collimating slit size are seen in the backprojection results shown in Figs. C-3 and C-4 where the 0° radial scans are presented. The ring source was smeared appreciably as the slit size increased. The width of the uniform source decreased slightly (~10 percent) as the slit width increased from 0.0127 to 0.127 cm. A similar effect is seen in the results of the ring source (Fig. C-4), with a 10 percent smearing of the inner region of the source.

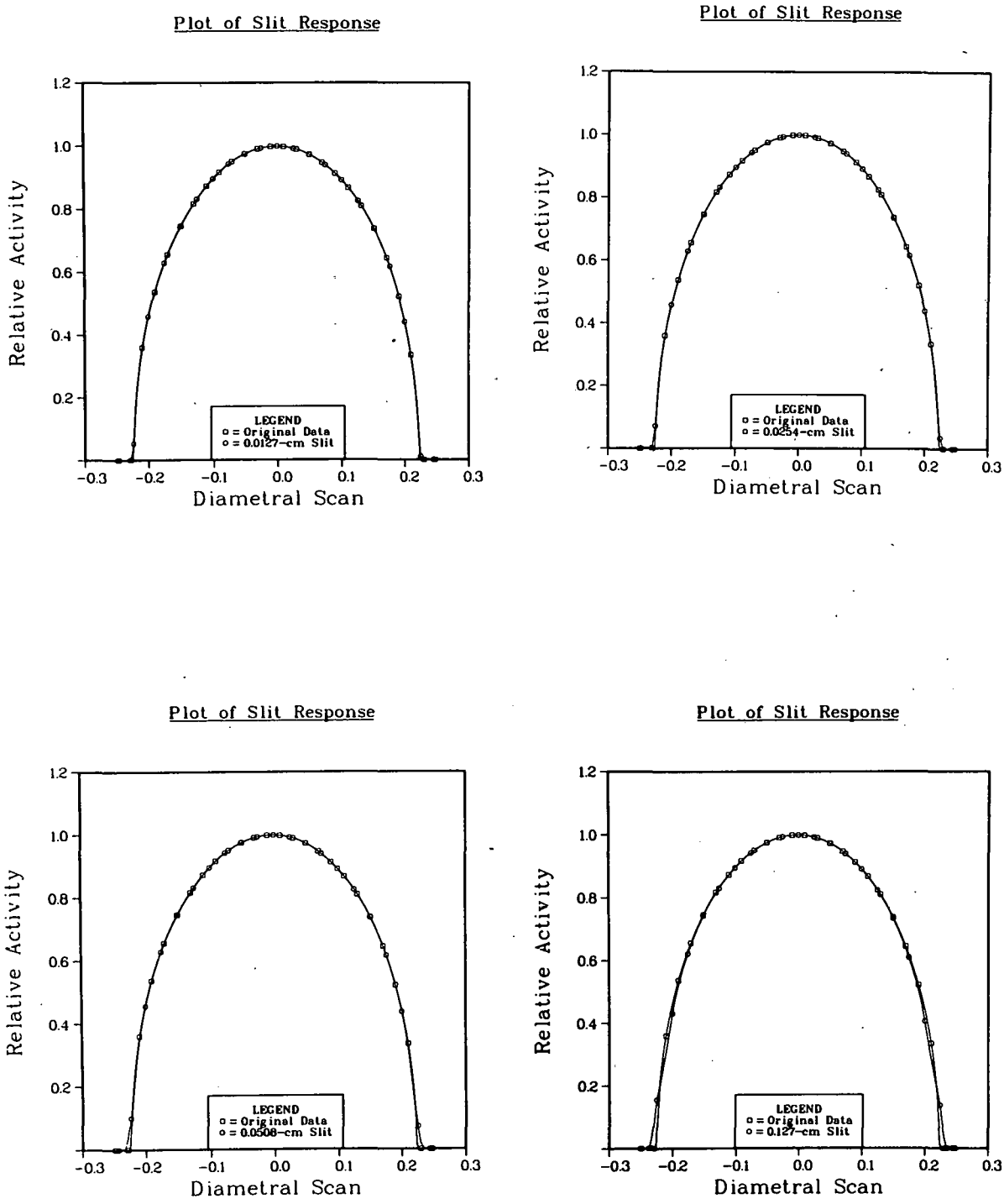

Figure C-1. Projections of a uniform source using various collimating slits.

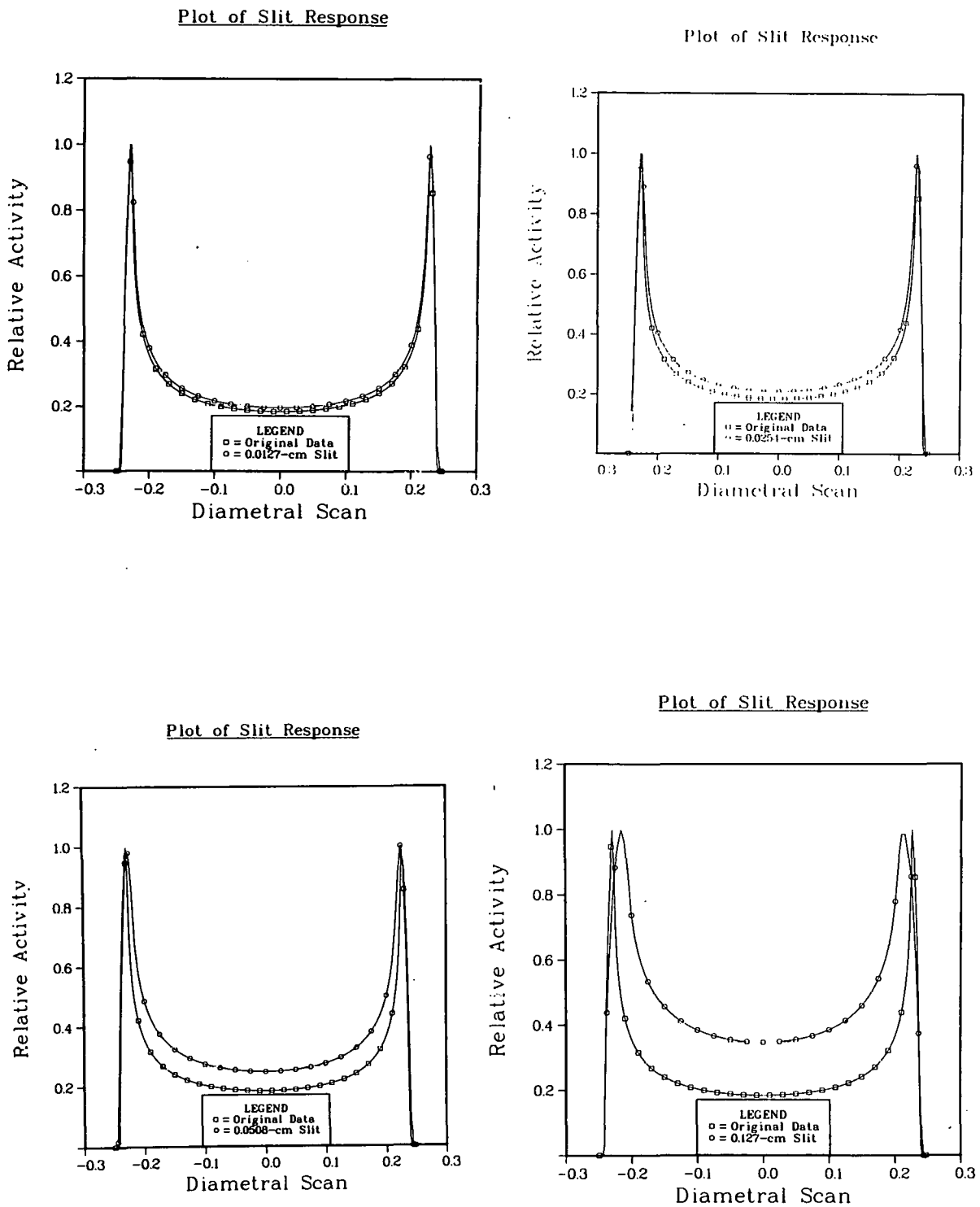

Figure C-2. Projections of a ring source using various collimating slits.

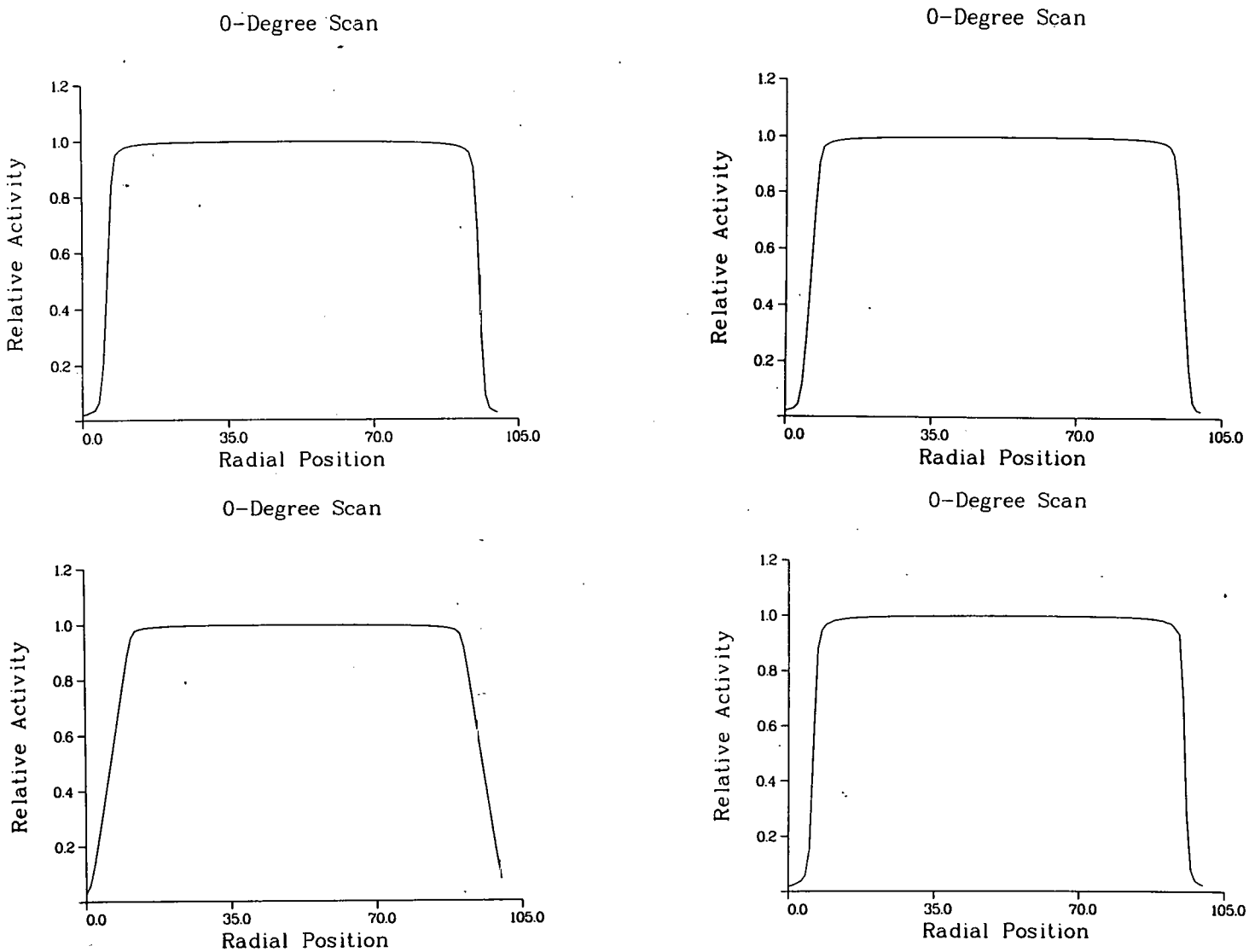

Figure C-3. Radial scans of the reconstructed images described in Fig. C-1 using the filtered backprojection technique.

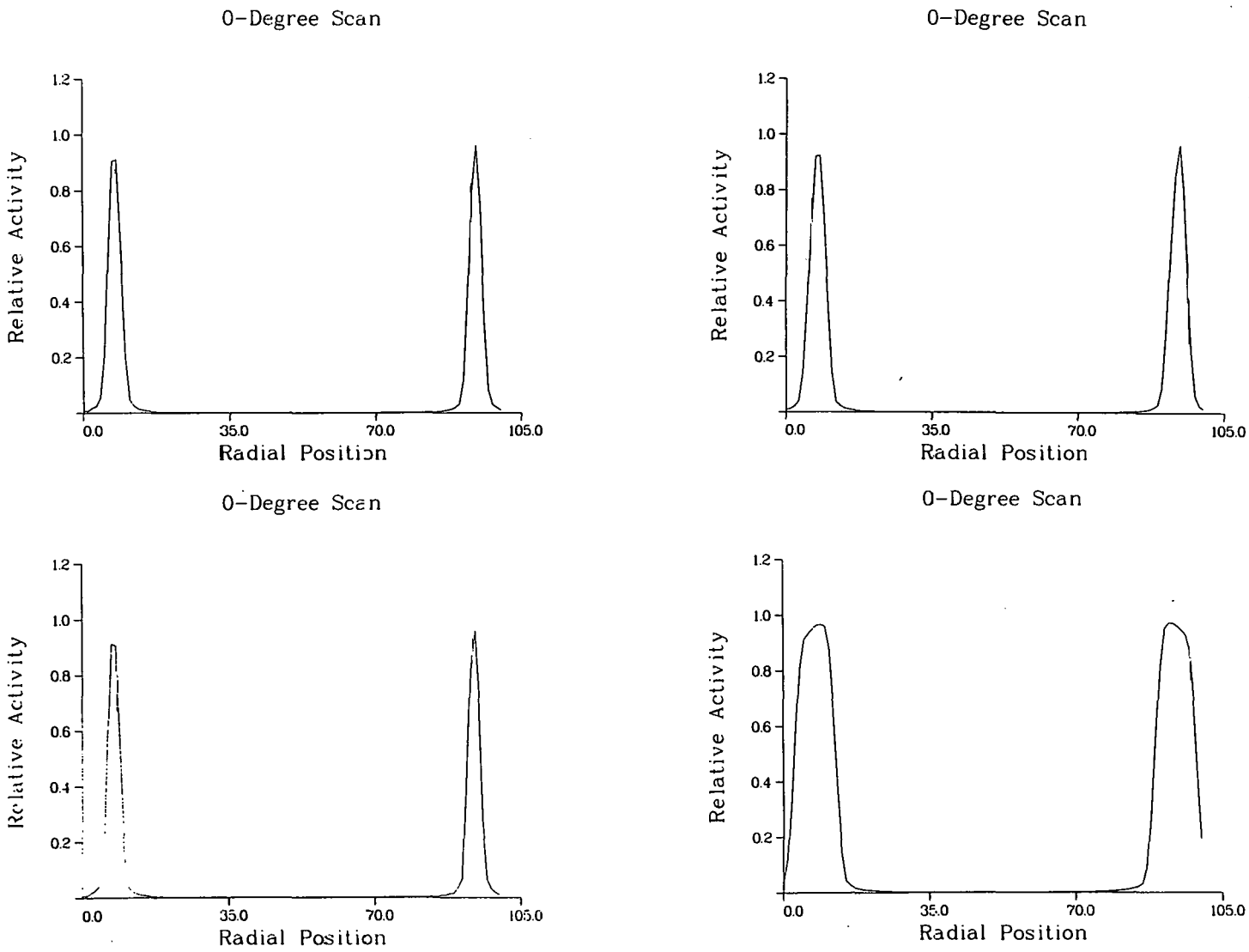

Figure C-4. Radial scans of the reconstructed images described in Fig. C-2 using the filtered backprojection technique.

APPENDIX D

COMPARISON OF FOUR RECONSTRUCTION AND UNFOLDING TECHNIQUES

Four techniques to reconstruct an image from a small number of projections were compared experimentally. These are filtered backprojections, Fourier Transforms Technique (TOMO)(22), a multiplicative algebraic iterative reconstruction technique (MART)(18), a recent adaptation of the algebraic reconstruction technique (ART) to a maximum entropy (MENT) criterion, and the unfolding technique (TWODIM) developed at Los Alamos (3,4).

The reconstruction of a picture from its projections is a highly indeterminate problem. Particularly for a small number of projections, one can only obtain an approximation of the original distribution function. It has been proved that, even for ideal cases, a nontrivial picture cannot be uniquely determined from a finite set of its projections (9-11). Thus, reconstruction techniques are heuristic, and an analytical estimate of their performance is difficult. The most reasonable evaluation technique is to qualitatively and quantitatively compare the performance of the algorithms for typical sets of data characteristics of the particular problem of interest.

For the comparison of the four techniques, we used the test case described in Section 4, Results (a combination of a skewed uniform source plus a skewed ring source). The results are shown in Figs. D-1 through D-4 with two radial scans and the isometric projection presented. The version of MART used in this investigation was set up to handle only three projections as input, hence, the hexagonal reconstruction was to be expected. The radial scans indicate that MART was not providing a reasonable reconstruction.

The MENT algorithm reconstructed the original image reasonably well as is shown in Fig. D-3; however, it failed to accurately reconstruct some of the other test cases. It also has a tendency to introduce ring artifacts in reconstruction that should be uniform. MENT also has a distinct disadvantage in that it requires about four times as long to compute the reconstruction.

TWODIM reconstruction results (Fig. D-4) are reasonable, but the radial scans are smeared by the volume averaging technique used in the code.

Based upon these results, filtered backprojection was selected as the preferable reconstruction technique for determining the two-dimensional distribution of fission products in fuel rods.

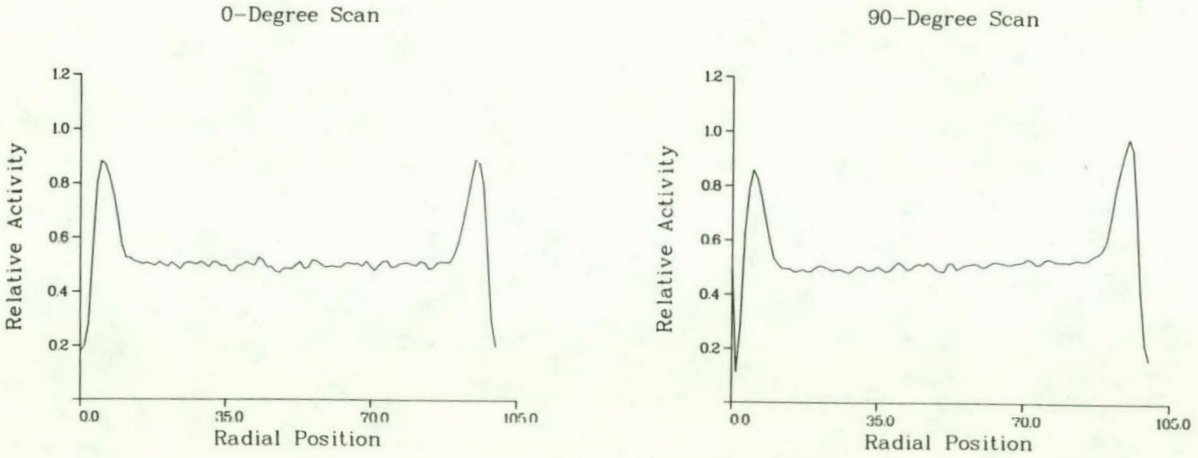

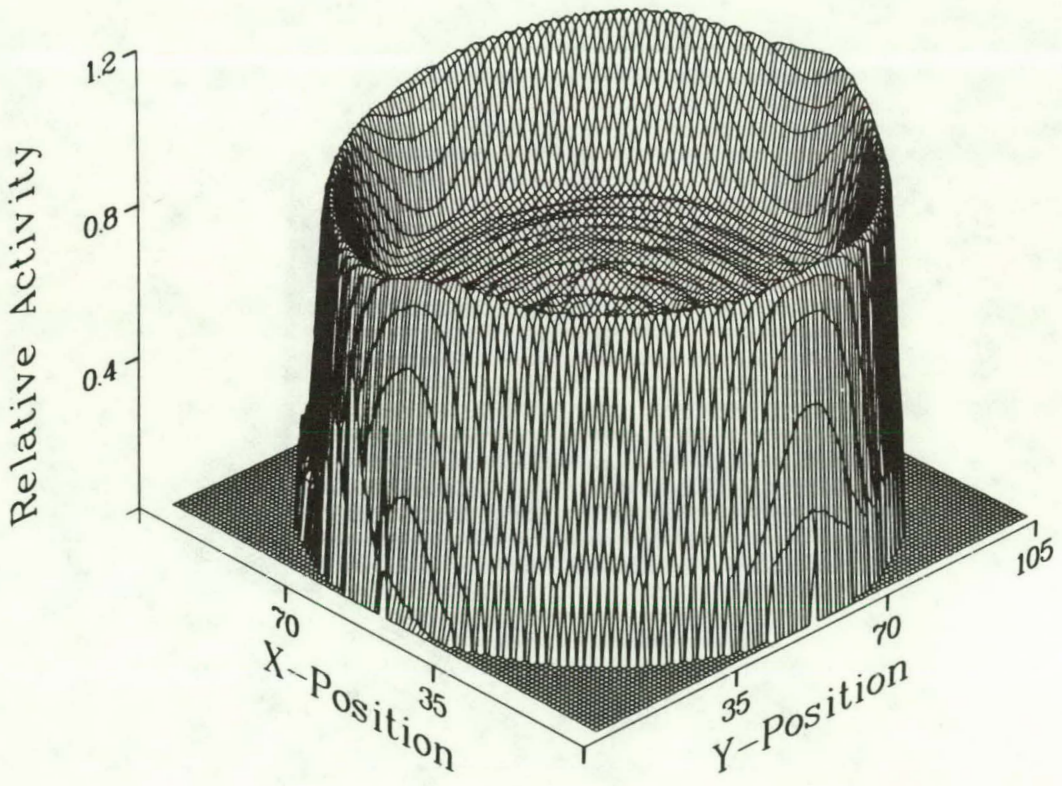

Figure D-1. Backprojection reconstruction for the simulated gamma-ray source (TOMO).

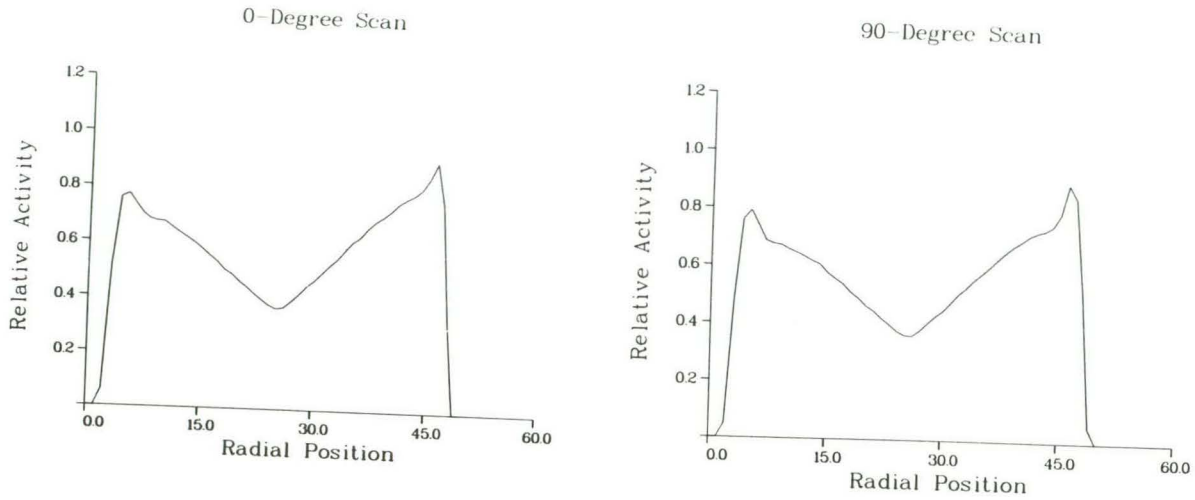

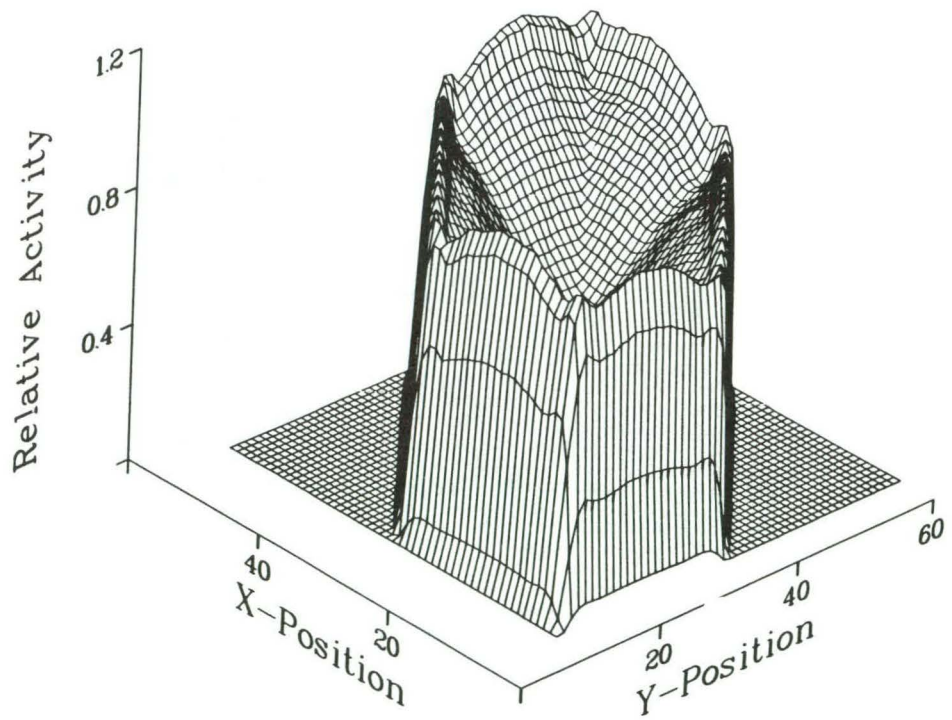

Figure D-2. Multiplicative adaptation of ART for the simulated gamma-ray source (MART).

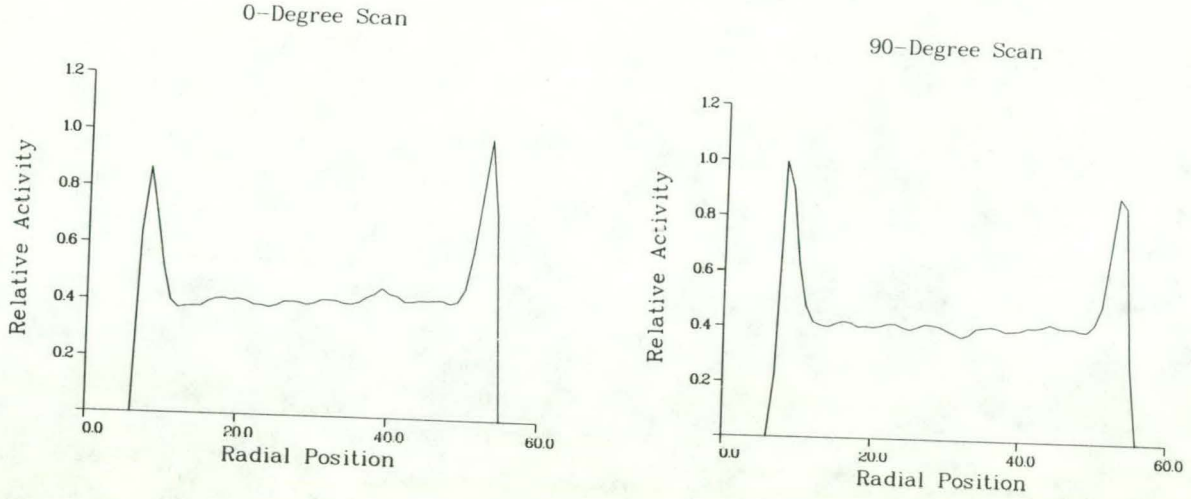

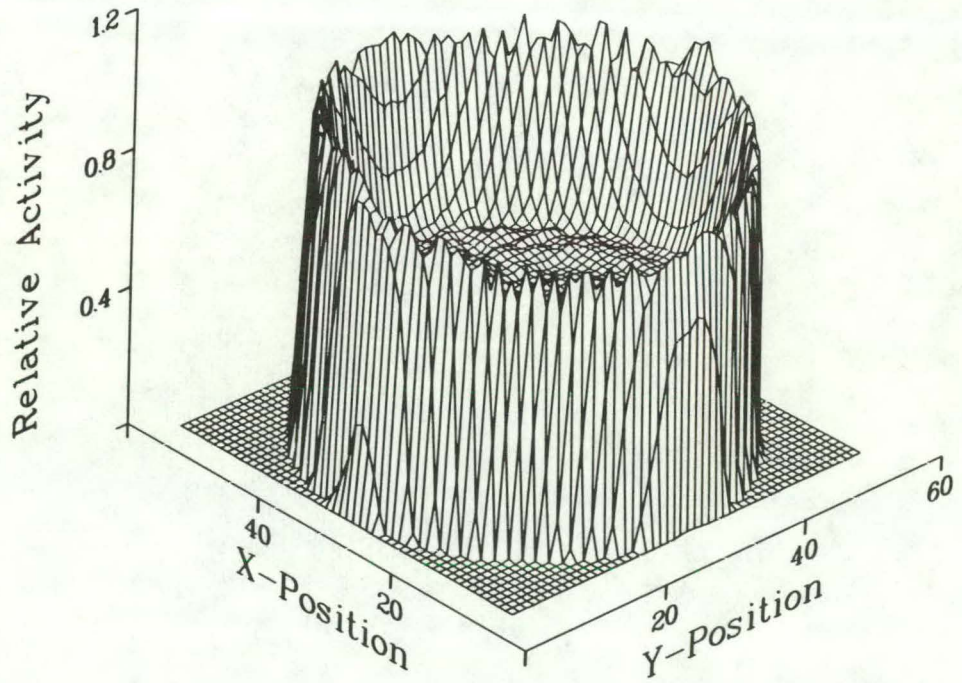

Figure D-3. Maximum entropy reconstruction for the simulated gamma-ray source (MENT).

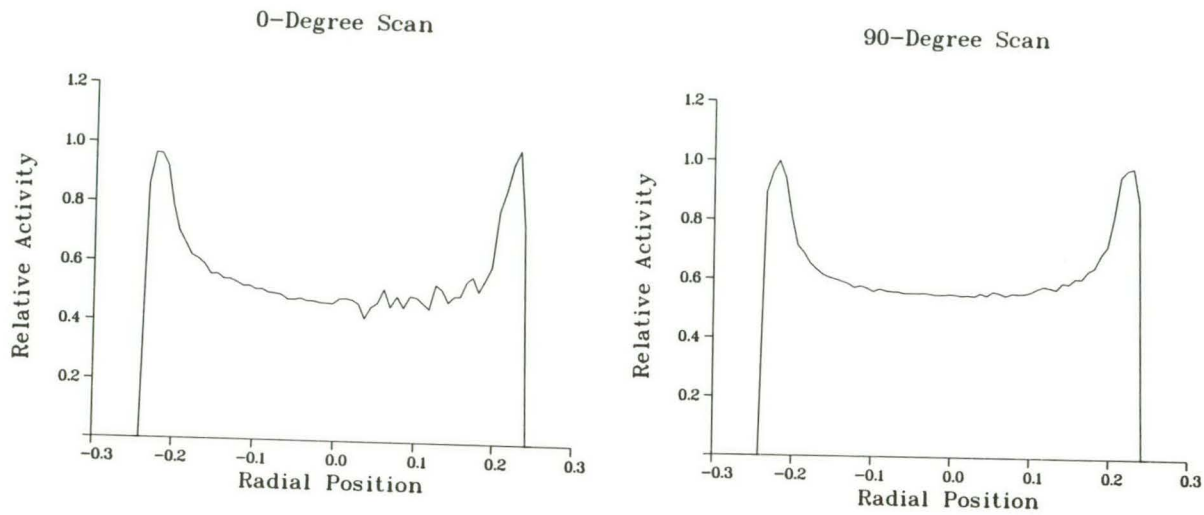

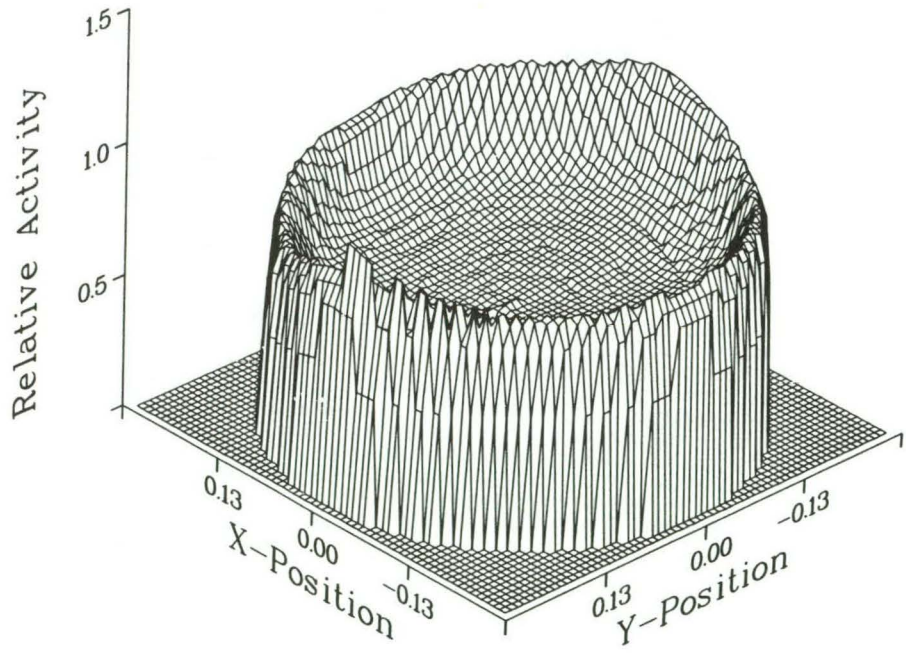

Figure D-4. Unfolded reconstruction for the simulated gamma-ray source (TWODIM).

REFERENCES

1. D. M. Holm, W. M. Sanders, J. L. Parker, H. D. Cowan, "Examination of Fast Reactor Fuel Elements with a Ge(Li) Anticoincidence Gamma-Ray Spectrometer," Proc. 16th Conf. Remote Syst. Technol., 228-242 (1969).

2. J. R. Phillips, "New Techniques in Precision Gamma Scanning: Application to Fast-Breeder Reactor Fuel Pins," Los Alamos National Laboratory report LA-5260-T (July 1973).

3. B. K. Barnes, J. R. Phillips, "TWODIM: A Computer Code for Unfolding Diametral Gamma-Ray Scans of Reactor Fuel Elements," Los Alamos National Laboratory report LA-4676 (May 1971).

4. J. R. Phillips, "Improved Nondestructive Determination of Two-Dimensional Radial Isotopic Distribution in Irradiated Fuel Pins," Nucl. Technol., Vol. 28, 282-290 (February 1976).

5. N. H. Abel, J. Reine Angen. Math. 1, 153-157 (1826).

6. Radon, J. Ober die Bestimmung von Funktionen durch ihre integralwerte langs gewisser Mannigfaltigkeiten (On the determination of functions from their integrals along certain manifolds). Ber. Saechs. Akad. Wiss. Leipzig, Math.-Phys. Kl. 69, 262-277 (1917).

7. G. T. Herman, Image Reconstruction From Projections, Vol. 32, Springler-Verlag, Berlin-Heidelberg (1979).

8. D. Ludwig, "The Radon Transform on Euclidean Space," Comm. Pure Appl. Math., 19, 49-81 (1966).

9. G. T. Herman, "Two Direct Methods for Reconstructing Pictures from Their Projections: A Comparative Study," Comput. Graphics Image Process 1 (2), 123-144 (1971).

10. K. T. Smith, D. C. Solmon, S. L. Wagner, "Practical and Mathematical Aspects of the Problem of Reconstructing Objects from Radiographs," Bull. Amer. Math. Soc., 23, No. 6, 1227-1270 (November 1977).

11. M. B. Katz, "Questions of Uniqueness and Resolution in Reconstruction of 2-D and 3-D Objects from Their Projections," Dissertation, Mathematical Department, University of California, Berkeley, Calif. (1976).

12. T. F. Budinger, G. T. Gullberg, "Three Dimensional Reconstruction in Nuclear Medicine by Iterative Least-Squares and Fourier Transform Techniques," Lawrence Berkeley Laboratory report LBL-2146 (January 1974).

13. G. T. Herman and S. Rowland, "Three Methods for Reconstructing Objects from X-Rays: A Comparative Study," Comput. Graphics and Image Process 2, 151-178 (1973).

14. W. Swindell, H. H. Barrett, "Computerized Tomography: Taking Section X-Rays," Physics Today, Vol. 30, No. 2, 32-41 (December 1977).

15. R. Gordon and G. T. Herman, "Reconstruction of Pictures from Their Projections," Commun. ACM 14 (12), 759-768 (1971).

16. G. T. Herman, A. Lent, and S. Rowland, "ART: Mathematics and Applications (A Report on the Mathematical Foundations and on the Applicability to Real Data of the Algebraic Reconstruction Techniques)," J. Theor. Biol. 42(1), 1-32 (1973).

17. R. Gordon, "A Tutorial on ART (Algebraic Reconstruction Techniques)," IEEE Trans. Nucl. Sci., in press.

18. G. N. Minerbo and J. G. Sanderson, "Reconstruction of a Source from a Few (2 or 3) Projections," Los Alamos National Laboratory report LA-6747-MS (1977).

19. R. Gordon, R. Bender, G. T. Herman, "Algebraic Reconstruction Techniques (ART) for Three-Dimensional Electron Microscopy and X-Ray Photography," J. Theor. Biol. 29, 471-481 (1970).

20. G. N. Minerbo, "MENT: A Maximum Entropy Algorithm for Reconstructing a Source from Projection Data," Computer Graphics and Image Processing 10, 48-68 (1979).

21. B. K. Barnes, J. R. Phillips, G. R. Waterbury, J. N. Quintana, A. S. Murray, J. R. Netuschil, "Computer Analysis and Control for Nondestructive Gamma Scanning of LMFBR Fuel Pins," presented at the ANS Conference on Computers in Activation Analysis and Gamma-Ray Spectroscopy, Mayaguez, Puerto Rico, April 30-May 3, 1978, published in Computer in Activation Analysis and Gamma-Ray Spectroscopy, Editors B. S. Carpenter, M. D. D'Agostino, H. P. Yule, DOE Publication (1979).

22. TOMO, written by Mike Cannon, M-8, Los Alamos National Laboratory, Private communication (1980).

23. R. Gordon and G. T. Herman, "Three-Dimensional Reconstruction from Projections: A Review of Algorithms," Int. Rev. Cytol., 111-131 (1973).

24. G. T. Herman and R. M. Lewitt, "Overview of Image Reconstruction from Projections," Topics in Applied Physics 32, 1-7, edited by G. T. Herman (1979).

25. Core Design and Operating Data for Cycles 1 and 2 of Quad Cities I, Electric Power Research Institute report EPRI NP-240 (November 1976).

26. J. R. Phillips, G. R. Waterbury, N. E. Vanderborgh, "Distributions of ^{134}Cs and ^{137}Cs in the Axial Blankets of Irradiated (U, Pu)O_2 Fuel Pins," J. Inorg. Chem., 1974, Vol. 367, pp. 17-23 (January 1974).

27. Los Alamos National Laboratory Group X-6, "MCNP - A General Monte Carlo Code for Neutron and Photon Transport," Los Alamos National Laboratory report LA-7396-M (November 1979).